2010-07-09

Real-Space Approach to Time Dependent Current Density Functional Theory

Daniel S. Jensen
Brigham Young University - Provo

Real-space Time-domain Approach to Time Dependent Current Density Functional Theory

Daniel Spencer Jensen

A thesis submitted to the faculty of
Brigham Young University
in partial fulfillment of the requirements for the degree of

Master of Science

Bret C. Hess, Chair
Harold T. Stokes
Gus Hart

Department of Physics and Astronomy

Brigham Young University

August 2010

ABSTRACT

Real-space Time-domain Approach to Time Dependent

Current Density Functional Theory

Daniel Spencer Jensen

Department of Physics and Astronomy

Master of Science

A real-space time-domain calculation of the frequency-dependent dielectric constant of nonmetallic crystals is outlined and the integrals required for this calculation are computed. The outline is based on time dependent current density functional theory and is partially implemented in the *ab initio* density functional theory FIREBALL program. The addition of a vector potential to the Hamiltonian of the system is discussed as well as the need to include the current density in addition to the particle density. The derivation of gradient integrals within a localized atomic-like orbital basis is presented for use in constructing the current density. Due to the generality of the derivation we also give the derivation of the kinetic energy, dipole, and overlap interactions.

Keywords: Time dependent current density functional theory, molecular integrals

ACKNOWLEDGMENTS

A special thanks to Dr. Bret Hess for all of his mentoring, support, and patience. I thank Dr. James P. Lewis for permission to use and modify the FIREBALL program. I especially thank my dear wife Becky for her incredible patience and support.

Contents

List of Figures

Chapter 1

Introduction

The response of materials to electromagnetic fields is a central problem in physics and is the main focus of this thesis. We describe herein a method for calculating the response of non-metallic solids to oscillating optical frequency electromagnetic fields. Such solids generally exhibit a macroscopic response to these fields and our goal is to predict this response to aid in the design of photovoltaics and other devices based on light absorption.

The method that we outline in this thesis is based on the macroscopic Maxwell equations in combination with time-dependent current density functional theory (TDCDFT). We use TDCDFT as presented by Ghosh and Dhara [1] to find the physical electric current density and electric field present in the solid. It has been shown that this theory is necessary when modeling periodic systems using density functional theory (DFT). [2] Our particular method is performed in the time domain with a local-orbital basis. It uses Fourier transforms after the simulation is performed to compute the desired optical properties as functions of frequency. This is in contrast to a previous TDCDFT implementation by Kootstra et al., [3] which is a linear response method that switches to the frequency domain early in the calculation. In this thesis we describe our proposed TDCDFT method and present the derivation of the molecular integrals needed for its implementation. We conclude the thesis with several

plots of these molecular integrals and a short discussion of the properties of our proposed TDCDFT method.

In this introduction we describe the macroscopic Maxwell equations and discuss a definition of polarization that can be applied to extended matter. The optical properties of solids such as the dielectric function and susceptibility can then be computed using a relationship between this polarization and the macroscopic electric field. We discuss the need to use approximate solutions to the Schrödinger equation in order to find the electric charge and current density for use in the macroscopic Maxwell equations. In particular, we focus on the use of TDCDFT to obtain this charge and current density.

1.1 Maxwell's Equations and Polarizability

The macroscopic Maxwell equations

$$\boldsymbol{\nabla} \cdot \boldsymbol{B} = 0, \qquad \boldsymbol{\nabla} \times \boldsymbol{E} + \frac{\partial \boldsymbol{B}}{\partial t} = 0, \tag{1.1a}$$

$$\boldsymbol{\nabla} \cdot \boldsymbol{D} = \rho_{\text{ext}}, \qquad \boldsymbol{\nabla} \times \boldsymbol{H} - \frac{\partial \boldsymbol{D}}{\partial t} = \boldsymbol{J}_{\text{ext}}, \tag{1.1b}$$

describe the macroscopic response of matter to electromagnetic waves. These equations and all others in this thesis are written in SI units unless mentioned otherwise. The term 'macroscopic' here refers to distances larger than 100 Å as explained in Ref. [4, Pg. 249]. In these equations, ρ_{ext} and $\boldsymbol{J}_{\text{ext}}$ are the charge and current densities external to the solid while $\boldsymbol{D}$ and $\boldsymbol{H}$ are macroscopic fields whose components are related to the averaged microscopic electric and magnetic fields $\boldsymbol{E}$ and $\boldsymbol{B}$ by the equations

$$D_\alpha = \epsilon_0 E_\alpha + P_\alpha - \Sigma_\beta \frac{\partial Q'_{\alpha\beta}}{\partial x_\beta} + \cdots, \tag{1.2}$$

$$H_\alpha = \frac{1}{\mu_0} B_\alpha - M_\alpha + \cdots. \tag{1.3}$$

In most materials we only need to include the macroscopically averaged electric and magnetic dipole moments $\boldsymbol{P}$ and $\boldsymbol{M}$ as the higher order moments are negligible, provided that the

frequencies are not too high [5, Pg. 61] and the material is not undergoing bulk motion [4, Pg. 256].

Unfortunately we cannot solve the macroscopic Maxwell equations (1.1) until we have some relation that allows us to write $\boldsymbol{D}$ and $\boldsymbol{H}$ in terms of $\boldsymbol{E}$ and $\boldsymbol{B}$. Such a relation is called a constitutive relation and can in general be complex (containing real and imaginary parts), nonlinear, nonlocal, and depend on temperature, pressure, past history, etc. [4, 6] In this thesis we assume that the following linear and local constitutive relation holds for $\boldsymbol{D}$:

$$D_\alpha(\boldsymbol{r},t) = \sum_\beta \int^t dt'\, \epsilon_0\, \epsilon_{\alpha\beta}(t-t')\, E_\beta(\boldsymbol{r},t')\,, \tag{1.4}$$

where $\epsilon_{\alpha\beta}(t-t')$ is a tensor called the macroscopic dielectric function and $\boldsymbol{E}$ is the macroscopic electric field. Equation (1.4) is a convolution and upon taking the Fourier transform in time of both sides we have:

$$D_\alpha(\boldsymbol{r},t) = \sum_\beta \epsilon_0\, \epsilon_{\alpha\beta}(\omega)\, E_\beta(\boldsymbol{r},\omega)\,. \tag{1.5}$$

Applying this constitutive relation to Eq. 1.2 and ignoring the electric quadrupole and higher densities we have the following relation for the macroscopic polarization:

$$P_\alpha(\boldsymbol{r},\omega) = \sum_\beta \chi_{\alpha\beta}(\omega)\, E_\beta(\boldsymbol{r},\omega)\,, \tag{1.6}$$

where χ is a tensor called the macroscopic susceptibility, which has the following relation to the dielectric function:

$$\epsilon_{\alpha\beta} = \epsilon_0\,(1+\chi_{\alpha\beta})\,. \tag{1.7}$$

In order to use the constitutive relation described above for solving Maxwell's equations, we need a definition of the macroscopic electric polarization $\boldsymbol{P}$. This is usually defined to be the average dipole moment per unit volume,

$$\boldsymbol{P}(\boldsymbol{r},t) = \frac{1}{\Omega_{\boldsymbol{r}}} \int^t dt' \int_\Omega d\boldsymbol{r}'\, \boldsymbol{r}'\rho_{\text{int}}(\boldsymbol{r}',t')\,, \tag{1.8}$$

where $\Omega_{\boldsymbol{r}}$ is a macroscopic volume representative of the solid and ρ_{int} is the charge density internal to the solid. (See Ref. [3, Pg. 6518] for a more thorough description of $\Omega_{\boldsymbol{r}}$ in terms of the applied fields and size of the unit cells.) This definition can work for some ionic or molecular solids where the electronic charge can be attributed to particular atoms in the unit cell but not so well in covalent crystals where important parts of the charge are between the atoms. (For more details on the failures of this and other classical definitions see Ref. [5, Pgs. 120-1].) Instead we use the definition,

$$\boldsymbol{P}(\boldsymbol{r},t) = -\frac{1}{\Omega_{\boldsymbol{r}}}\int^{t} dt' \int_{\Omega} d\boldsymbol{r}'\, \boldsymbol{j}_{\text{int}}(\boldsymbol{r}',t') \tag{1.9}$$

where $\boldsymbol{j}_{\text{int}}$ is the current density internal to the solid. This definition reduces to Eq. (1.8) when the charges can be attributed to particular atoms.

There is just one missing component left for solving the macroscopic Maxwell equations and that is the determination of the internal electric charge and current densities ρ_{int} and $\boldsymbol{j}_{\text{int}}$. An accurate description of these densities for materials that are covalently bonded requires quantum mechanical calculations since covalent bonding is inherently quantum mechanical. [7, Pg. 22] We proceed by studying the Schrödinger equation and show how its (approximate) solution gives us an accurate internal current density for use in Eq. (1.9).

1.2 Schrödinger Equation and Approximations

The nonrelativistic multiatom Schrödinger equation is

$$i\hbar\frac{\partial\Psi}{\partial t} = H\Psi, \tag{1.10}$$

where

$$H = \overbrace{\sum_{i=1}^{N} \frac{p_i^2}{2m_e}}^{T_\mathrm{e}} + \overbrace{\sum_{n=1}^{K} \frac{P_n^2}{2M_n}}^{T_\mathrm{n}} + \overbrace{\frac{1}{4\pi\epsilon_0} \sum_{i=1}^{N} \sum_{j>i}^{N} \frac{e^2}{|\boldsymbol{r}_i - \boldsymbol{r}_j|}}^{V_\mathrm{ee}} + \overbrace{\frac{1}{4\pi\epsilon_0} \sum_{n=1}^{K} \sum_{i=1}^{N} \frac{-Z_n e^2}{|\boldsymbol{r}_i - \boldsymbol{R}_n|}}^{V_\mathrm{en}} + \overbrace{\frac{1}{4\pi\epsilon_0} \sum_{n=1}^{K} \sum_{n'>n}^{K} \frac{Z_n Z_{n'} e^2}{|\boldsymbol{R}_n - \boldsymbol{R}_{n'}|}}^{V_\mathrm{nn}} \tag{1.11}$$

is the Hamiltonian of the system in the absence of any applied electromagnetic fields. [8, Pg. 44] This equation describes the time evolution of a system of N electrons and K nuclei where m_e is the mass of an electron, M_n is the mass of the n$^{\text{th}}$ nucleus, Z_n is the charge of the n$^{\text{th}}$ nucleus, $\boldsymbol{R}_n$ is the position of the n$^{\text{th}}$ nucleus, and $\boldsymbol{r}_i$ stands for the position and spin coordinates of the i$^{\text{th}}$ electron.[1] The term T_e is the kinetic energy of the electrons, T_n is the kinetic energy of the nuclei, V_ee is the electron-electron potential energy, V_en is the electron-nucleus potential energy, and V_nn is the nucleus-nucleus potential energy. The function $\Psi\left(\boldsymbol{r}_1, \ldots, \boldsymbol{r}_N, \boldsymbol{R}_1, \ldots, \boldsymbol{R}_K, t\right)$ is called the wave function for this system and it tells us everything that can be known about the system at time t. [9, Pg. 28] In particular, it can be used to find the correct electric charge and current density for use in the macroscopic Maxwell equations as presented in Sec. 2.2.

Unfortunately, closed-form solutions to Eq. (1.10) are not available for systems even as simple as the helium atom [9, Pg. 478] and for larger systems the solution is simply intractable. It should also be noted that the Hamiltonian in Eq. (1.11) doesn't account for any applied electric or magnetic fields, which can dramatically complicate the problem by bringing in time-dependent electromagnetic scalar and vector potentials. Evidently some approximations need to be made in order to solve this equation for multiatom systems.

[1] A careful derivation of any theory in electronic structure must explicitly keep track of the spin coordinate but to simplify our presentation we will neglect spin in the remainder of this thesis.

1.2.1 Calculus of Variations

Most of the approximations to the Schrödinger equation rely heavily on a mathematical tool called the calculus of variations. Using the calculus of variations, Dirac and Frenkel developed a variational principle known as the Dirac-Frenkel variational principle for approximately solving Eq. (1.10). The main result of this variational principle is that a trial wave function Ψ_{trial} depending on a set of parameters can be used to form an equation of motion that has a solution which approximates the exact solution of Eq. (1.10). Furthermore, as the parametrisation is improved, the solution from these equations of motion will approach the exact solution to within a given error bound. [10, Pg. 674] This variational principle is very important in numerical treatments of quantum dynamics and is applicable even in the presence of applied electromagnetic fields.

1.2.2 Born-Oppenheimer Approximation

A very important application of the variational principle to Eq. (1.10) is the Born-Oppenheimer approximation. To simplify our description of this approximation we will continue to exclude the effects of applied electromagnetic fields although they can be included as explained in Sec. 1.2.1. By excluding these fields we can perform separation of variables on Eq. (1.10) and work with just the time-independent Schrödinger equation,

$$H\Psi = E\Psi. \tag{1.12}$$

Eq. (1.12) yields a set of eigenvalues E_k and eigenfunctions Ψ_k such that the general solution can be written as

$$\Psi = \sum_k c_k \exp\left(-\frac{\imath}{\hbar} E_k t\right) \Psi_k, \tag{1.13}$$

where the c_k can be found by using the initial conditions of our system. [9, Pgs. 42-44]

At the heart of the Born-Oppenheimer approximation is the assumption that the wave function can be written as the product of a nuclear and electronic wave function with the

electronic wave function depending only parametrically on the positions of the nuclei,

$$\Psi\left(\boldsymbol{r}_1,\ldots,\boldsymbol{r}_N,\boldsymbol{R}_1,\ldots,\boldsymbol{R}_K\right)=\Phi\left(\boldsymbol{r}_1,\ldots,\boldsymbol{r}_N;\,\boldsymbol{R}_1,\ldots,\boldsymbol{R}_K\right)\Theta\left(\boldsymbol{R}_1,\ldots,\boldsymbol{R}_K\right), \tag{1.14}$$

where variables after the semicolons are fixed parameters. Using this approximation to replace Ψ in Eq. (1.11) we have the following pair of equations

$$H_{\text{elec}}\Phi\left(\boldsymbol{r}_1,\ldots,\boldsymbol{r}_N;\,\boldsymbol{R}_1,\ldots,\boldsymbol{R}_K\right)=E_e\left(;\boldsymbol{R}_1,\ldots,\boldsymbol{R}_K\right)\Phi\left(\boldsymbol{r}_1,\ldots,\boldsymbol{r}_N;\,\boldsymbol{R}_1,\ldots,\boldsymbol{R}_K\right), \tag{1.15}$$

where H_{elec} is the electronic Hamiltonian

$$H_{\text{elec}}=\overbrace{\sum_{i=1}^{N}\frac{p_i^2}{2m_e}}^{T_{\text{e}}}+\overbrace{\frac{1}{4\pi\epsilon_0}\sum_{i=1}^{N}\sum_{j>i}^{N}\frac{e^2}{|\boldsymbol{r}_i-\boldsymbol{r}_j|}}^{V_{\text{ee}}}+\overbrace{\frac{1}{4\pi\epsilon_0}\sum_{n=1}^{K}\sum_{i=1}^{N}\frac{-Z_ne^2}{|\boldsymbol{r}_i-\boldsymbol{R}_n|}}^{V_{\text{en}}} \tag{1.16}$$

and

$$H_{\text{nuc}}\Theta\left(\boldsymbol{R}_1,\ldots,\boldsymbol{R}_K\right)=E_n\Theta\left(\boldsymbol{R}_1,\ldots,\boldsymbol{R}_K\right), \tag{1.17}$$

where H_{nuc} is the nuclear Hamiltonian

$$H_{\text{nuc}}=\overbrace{\sum_{n=1}^{K}\frac{P_n^2}{2M_n}}^{T_{\text{n}}}+E_e+\overbrace{\frac{1}{4\pi\epsilon_0}\sum_{n=1}^{K}\sum_{n'>n}^{K}\frac{Z_nZ_{n'}e^2}{|\boldsymbol{R}_n-\boldsymbol{R}_{n'}|}}^{V_{\text{nn}}} \tag{1.18}$$

In deriving these equations we have neglected the following two terms,

$$-\Theta\left(\boldsymbol{R}_1,\ldots,\boldsymbol{R}_K\right)\sum_{n=1}^{K}\frac{1}{2M_n}\boldsymbol{\nabla}_{\boldsymbol{R}_n}^2\Phi\left(\boldsymbol{r}_1,\ldots,\boldsymbol{r}_N;\,\boldsymbol{R}_1,\ldots,\boldsymbol{R}_K\right) \tag{1.19a}$$

$$-\sum_{n=1}^{K}\frac{1}{M_n}\boldsymbol{\nabla}_{\boldsymbol{R}_n}\Theta\left(\boldsymbol{R}_1,\ldots,\boldsymbol{R}_K\right)\cdot\boldsymbol{\nabla}_{\boldsymbol{R}_n}\Phi\left(\boldsymbol{r}_1,\ldots,\boldsymbol{r}_N;\,\boldsymbol{R}_1,\ldots,\boldsymbol{R}_K\right), \tag{1.19b}$$

on the basis that they are small contributions as explained in Ref. [8, Pg. 81].

Simple justification for the Born-Oppenheimer approximation comes from the fact that the nuclei are much more massive than the electrons, ($m_n/m_e\approx 1839$ and $m_p/m_e\approx 1836$), and therefore move much slower on average. The result of this approximation as seen in Eqs. (1.15) and (1.17) is that we have a clear separation of the degrees of freedom of the electrons

from those of the nuclei. In the remainder of this thesis we will focus mainly on the solution of Eq. (1.15) while treating Eq. (1.17) only approximately as explained in Sec. 2.1. The main disadvantage to using the Born-Oppenheimer approximation is that electron-phonon couplings are neglected and their effects must be studied perturbatively when using this approximation.

1.2.3 Density Functional Theory

Although the Hamiltonian in Eq. (1.16) is greatly simplified over that of Eq. (1.11) it is still intractable due to the large number of degrees of freedom stemming from the V_{ee} term. There are several approaches that attack this problem by replacing this complicated term with an effective potential V_{eff} resulting in a Hamiltonian that is simply a sum of one-electron Hamiltonians,

$$H_{\text{IP}} = \sum_{i=1}^{N} \left[\overbrace{\frac{p_i^2}{2m_e}}^{T_{\text{e}}} + V_{\text{eff}}\left(\boldsymbol{r}_i;\, \boldsymbol{R}_1, \ldots, \boldsymbol{R}_k\right) + \overbrace{\frac{1}{4\pi\epsilon_0} \sum_{n=1}^{K} \frac{-Z_n e^2}{|\boldsymbol{r}_i - \boldsymbol{R}_n|}}^{V_{\text{en}}} \right] \tag{1.20}$$

where H_{IP} is called the 'independent-particle' Hamiltonian.[2] For a fictitious yet illustrative example of this replacement see Fig. 1.1. Some approaches, such as the Hartree-Fock approximation, achieve this replacement by treating the term approximately in a manner similar to the mean field theory approach of statistical mechanics. [8, Pg. 47] Other approaches, such as density functional theory and some post-Hartree-Fock methods, attempt to include all of the effects of V_{ee} in a systematic way while still using an independent-particle Hamiltonian. Although each approach has its advantages and disadvantages, we choose to focus on DFT due to its ability to handle very large numbers of electrons. It should be noted that the potential V_{eff} in Eq. (1.20) is, in general, a nonlocal operator that depends on the

[2]The V_{en} term in Eq. (1.20) is usually called the external potential V_{ext} in DFT and does not have to be the electron-nucleus interaction for DFT to be valid.

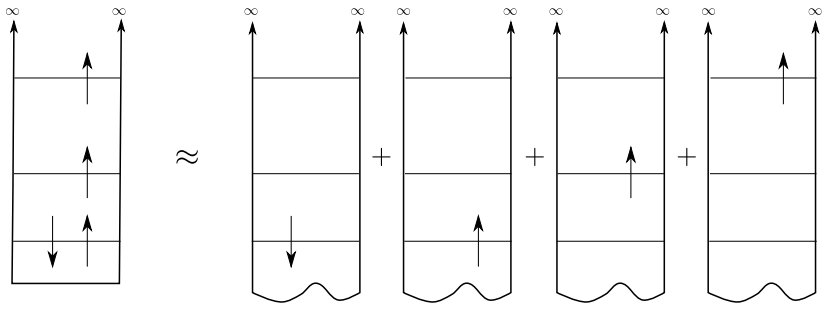

Figure 1.1 A 'many particles in a box' example of how a system of four interacting fermions can be split into four non-interacting one-body problems. Notice how each fermion in the noninteracting system has an effective potential based on the main square-well potential and the potential felt from the other fermions.

same wave function that it is acting upon and thus leads to a set of self-consistent equations characteristic of these approaches.

As mentioned above, DFT is particularly useful for solving Eq. (1.16) because it can be used to model large finite and periodic systems. (See Ref. [11, Ch. 23] for some examples of large systems including giant fullerenes and DNA molecules.) This is made possible mainly by working with the particle density

$$\rho(\boldsymbol{r}) = \frac{\langle \Phi | \hat{\rho}(\boldsymbol{r}) | \Phi \rangle}{\langle \Phi \mid \Phi \rangle} = N \frac{\int d\boldsymbol{r}_2 \cdots d\boldsymbol{r}_N \left| \Phi(\boldsymbol{r}, \boldsymbol{r}_2, \ldots, \boldsymbol{r}_N) \right|^2}{\int d\boldsymbol{r}_1 d\boldsymbol{r}_2 \cdots d\boldsymbol{r}_N \left| \Phi(\boldsymbol{r}_1, \boldsymbol{r}_2 \ldots, \boldsymbol{r}_N) \right|^2}, \tag{1.21}$$

where $\hat{\rho}(\boldsymbol{r}) = \sum_{i=1}^{N} \delta(\boldsymbol{r} - \boldsymbol{r}_i)$ is the density operator. [11, Pg. 54] Notice that $\rho(\boldsymbol{r})$ in Eq. (1.21) only depends on 3 spatial variables in comparison with the $3N$ spatial variables that the complicated many-body electronic wave function in Eq. (1.15) depends on. (Here we are still assuming that there are N electrons.) Note that the density ρ in Eq. (1.21) is called the particle density and must be multiplied by the charge of an electron e to convert it to the charge density in Maxwell's equations. Justification for this switch in focus from wave function to density comes from the Hohenberg-Kohn theorems described below.

The two Hohenberg-Kohn theorems developed in 1964 form the theoretical foundation

of DFT. [12] The main result of the first Hohenberg-Kohn theorem is that all properties of a system obeying Eq. (1.15) can be found using only the ground state density

$$\rho_0(\boldsymbol{r}) = \frac{\langle \Phi_0 | \hat{\rho}(\boldsymbol{r}) | \Phi_0 \rangle}{\langle \Phi_0 \mid \Phi_0 \rangle}, \tag{1.22}$$

where Φ_0 is the ground-state wave function. The main result of the second Hohenberg-Kohn theorem is that there exists a universal functional of the density $E[\rho]$ that can be with the exact ground-state energy. The density that minimizes this functional is the exact ground state density so by combining the two theorems we see that if we have the correct energy functional $E[\rho]$ then we have an *exact* theory of many-body systems appropriately named DFT. [11, Sec. 6.2] That such a functional exists was clarified later in the constrained search formulation of Levy and Lieb, which hinges on the ability to express the density in terms of an N-electron wave function and is commonly referred to as N-representability. [11, Pg. 126]

Although the Hohenberg-Kohn theorems provide a theoretical foundation for DFT, they do not describe a procedure for actually finding the functional $E[\rho]$ in the second Hohenberg-Kohn theorem. That procedure was provided by Kohn and Sham in 1965 [13] and is the reason why DFT has become such a powerful tool in electronic structure calculations. In this approach the functional in the second Hohenberg-Kohn theorem is written as[3]

$$E[\rho] = T_n[\rho] + \int d\boldsymbol{r}\, \rho(\boldsymbol{r})\, V_{\text{en}}(\boldsymbol{r}) + E_{\text{Hartree}}[\rho] + E_{\text{xc}}[\rho] \tag{1.23}$$

where T_{n} is the kinetic energy functional of a noninteracting electron gas, E_{Hartree} is the classical Coulomb interaction functional

$$E_{\text{Hartree}}[\rho] = \frac{1}{2}\frac{e^2}{4\pi\epsilon_0}\int d\boldsymbol{r}\int d\boldsymbol{r}'\frac{\rho(\boldsymbol{r})\,\rho(\boldsymbol{r}')}{|\boldsymbol{r}-\boldsymbol{r}'|} \tag{1.24}$$

[3]This energy functional is only well-defined for periodic systems if we add the ion-ion interaction energy functional to make the system neutral.

and E_{xc} is the exchange-correlation functional representing the energy from all correlation effects[4] and any other energy not accounted for in the other three terms.

Applying the calculus of variations to Eq. (1.23) results in the Kohn-Sham Schrödinger-like equations,

$$\left[-\frac{\hbar^2}{2m_e}\nabla^2 + V_{\text{eff}}(\boldsymbol{r})\right]\psi_k(\boldsymbol{r}) = \epsilon_k\psi_k(\boldsymbol{r}),\ k = 1,\ldots,N \tag{1.25}$$

where

$$V_{\text{eff}}(\boldsymbol{r}) = V_{\text{en}}(\boldsymbol{r}) + V_{\text{xc}} + \frac{e^2}{4\pi\epsilon_0}\int d\boldsymbol{r}'\,\rho(\boldsymbol{r}')\,\frac{1}{|\boldsymbol{r}-\boldsymbol{r}'|}, \tag{1.26}$$

and $V_{\text{xc}} = \frac{\delta E_{\text{xc}}[\rho]}{\delta\rho(\boldsymbol{r})}$ is the exchange-correlation potential. These equations are of the desired independent-electron form shown in Eq. (1.20) but must be solved self-consistently since the potential V_{eff} depends on the density, which in turn depends on the unknown independent-electron wave function. As seen in Eqs. (1.25) and (1.26), the Kohn-Sham approach rests on the assumption that the true ground-state electron density can be written as the density of an independent-electron system.[5] This assumption is known as the Kohn-Sham *ansatz* and it remains to be proven for any real systems of interest. If the Kohn-Sham *ansatz* is true then the Kohn-Sham approach will, in principle, solve Eq. (1.15) exactly.

As mentioned above, the Kohn-Sham approach is in principle exact but in practice there are several important assumptions involved in actual calculations. By separating out the kinetic energy functional of the noninteracting gas and the long-range Hartree terms, it often becomes reasonable to approximate the exchange-correlation functional E_{xc} as a local functional of the density in what is called the local density approximation (LDA). There exist other approximations to the exchange-correlation functional that improve upon the LDA such as the generalized gradient approximation (GGA), hybrid functionals, orbital-dependent functionals, etc. (See Ref. [11, Ch. 8] for a review of these approximation schemes for the

[4]Exchange is just a special form of correlation stemming from the Pauli exclusion principle.

[5]The Kohn-Sham ansatz is often referred to in DFT literature as the non-interacting-V-representability question.

exchange-correlation functional.) Other approximations used in the Kohn-Sham approach depend on the particular implementation chosen. The three main implementations of the Kohn-Sham approach are plane wave and grid methods, localized atomic(-like) orbitals, and atomic sphere methods. These implementations are formally equivalent and a thorough description of them can be found in Ref. [11, Chs. 12-17].

1.2.4 Time Dependent (Current) Density Functional Theory

Our formulation of DFT in Sec. 1.2.3 deals only with the time-*independent* Schrödinger equation and therefore cannot model the effects of any time-dependent electromagnetic fields. As was mentioned in Sec. 1.2.1, the calculus of variations can be applied successfully to the time-*dependent* Schrödinger equation given in Eq. (1.10) so the question naturally arises: can the DFT formalism be extended to time-dependent phenomenon? That question was answered in 1984 with the development of the Runge-Gross theorem. [14] The Runge-Gross theorem is the theoretical basis for time-dependent density functional theory (TDDFT) much like the Hohenberg-Kohn theorems are the theoretical basis for DFT. The main result of this theorem is that there exists a one-to-one mapping between the time-dependent density $\rho(\boldsymbol{r}, t)$ and the many-body time-dependent *scalar* potentials in which the system is evolving.

The Runge-Gross theorem does not provide a method for actually computing the time development of a system much like the Hohenberg-Kohn theorems don't provide a method for applying DFT. Three computational methods for applying TDDFT were proposed in the original paper by Runge and Gross with the most commonly used method being an extension of the Kohn-Sham equations to time-dependent phenomenon. This method involves solving the independent-particle time-dependent Schrödinger-like equations,

$$i\hbar\frac{d\Phi_k(t)}{dt} = H(t)\,\Phi_k(t)\,,\; k = 1, \ldots, N \tag{1.27}$$

where

$$H(t) = \frac{p^2}{2m_e} - eV_{\mathrm{EM}}(t) + V_{\mathrm{ext}}(\boldsymbol{r}, t) + \frac{e^2}{4\pi\epsilon_0}\int d\boldsymbol{r}' \frac{\rho(\boldsymbol{r}', t)}{|\boldsymbol{r} - \boldsymbol{r}'|} + V_{\mathrm{xc}}[\rho](\boldsymbol{r}, t) \tag{1.28}$$

and a spatially-constant electric field is included in the scalar potential V_{EM}:

$$V_{\mathrm{EM}}(t) = \boldsymbol{E}_{\mathrm{ext}}(t) \cdot \boldsymbol{r} \tag{1.29}$$

In the Runge-Gross theorem the exchange-correlation potential V_{xc} seen in Eq. (1.28) is actually a functional of the density evaluated at all times t' previous to the current time t. [14, Eq. (14)] This added complication in TDDFT is currently its greatest weakness as we still do not have a useful universal functional of time. [11, Pg. 148] This problem is typically resolved by making the adiabatic local density approximation (ALDA) where this time dependence is simply ignored and the exchange-correlation potential from DFT is used instead.

The Kohn-Sham TDDFT method is usually implemented using either a linear response approach or a real-time approach. We choose to focus on the real-time approach as it is currently better than the linear response approach at modeling large systems. This advantage stems from the fact that only occupied states are propagated in the real-time approach whereas the linear response approach involves the creation and diagonalization of large matrices depending on the number of occupied and unoccupied orbitals. [11, Pg. 412] (These matrices are $N_{\mathrm{pair}} \times N_{\mathrm{pair}}$ in size where $N_{\mathrm{pair}} = 2N_{\mathrm{occupied}} \times N_{\mathrm{unoccupied}}$.) The real-time approach is also capable of modeling nonlinear phenomenon since it is not limited to small perturbations as in the linear response approach.

The form of the Hamiltonian in Eq. (1.28) is valid for finite systems subject to time-dependent electric fields but not for periodic systems or for systems subject to time-dependent magnetic fields. This Hamiltonian doesn't apply to periodic systems because the continuity equation is used at the end of the Runge-Gross theorem to relate the current density to the particle density and a certain surface integral involving the density is assumed to vanish.

This integral simply cannot be chosen to vanish in a periodic system with a uniform applied field. [2] This Hamiltonian is also inadequate for including time-dependent magnetic fields since it can only model fields that can be written in the scalar potential of Eq. (1.29).

Ghosh and Dhara show in Ref. [1] that the Runge-Gross theorem can be extended to model periodic systems and those subject to time-dependent magnetic fields. In this new theory called TDCDFT, the current density must be retained as a basic variable and the Hamiltonian is written as

$$H(t) = \frac{1}{2m_e}\left[\boldsymbol{p} + e\boldsymbol{A}_{\text{eff}}(\boldsymbol{r},t)\right]^2 - eV_{\text{eff}}(\boldsymbol{r},t), \tag{1.30}$$

where

$$\boldsymbol{j}(\boldsymbol{r},t) = \frac{\hbar}{m_e}\Im\left\{\sum_{k=1}^{N}\Phi_k^*(\boldsymbol{r},t)\,\boldsymbol{\nabla}\Phi_k(\boldsymbol{r},t)\right\} - \frac{e}{m_e}\boldsymbol{A}_{\text{eff}}\rho(\boldsymbol{r},t), \tag{1.31}$$

$$\boldsymbol{A}_{\text{eff}}(\boldsymbol{r},t) = \boldsymbol{A}_{\text{ext}}(\boldsymbol{r},t) + \frac{\mu_0 e}{4\pi}\int d\boldsymbol{r}'\,\frac{\boldsymbol{j}(\boldsymbol{r}',t)}{|\boldsymbol{r}-\boldsymbol{r}'|} + \frac{1}{ec}\frac{\delta E_{\text{xc}}}{\delta \boldsymbol{j}}, \text{ and} \tag{1.32}$$

$$\begin{aligned} V_{\text{eff}}(\boldsymbol{r},t) = V_{\text{en}}(\boldsymbol{r}) - eV_{\text{ext}}(\boldsymbol{r},t) + \frac{e^2}{4\pi\epsilon_0}\int d\boldsymbol{r}'\,\frac{\rho(\boldsymbol{r}',t)}{|\boldsymbol{r}-\boldsymbol{r}'|} \\ + \frac{\delta E_{\text{xc}}}{\delta\rho} + \frac{e^2}{2m_e}\left(\boldsymbol{A}_{\text{eff}}^2 - \boldsymbol{A}_{\text{ext}}^2\right) \end{aligned} \tag{1.33}$$

are the current density, effective vector potential, and effective scalar potential respectively. The effective vector and scalar potentials are the macroscopic potentials of the system and they are related to the macroscopic electromagnetic fields inside the material via the equations:

$$\boldsymbol{E}_{\text{eff}} = -\boldsymbol{\nabla}V_{\text{eff}} - \frac{\partial}{\partial t}\boldsymbol{A}_{\text{eff}} \text{ and} \tag{1.34}$$

$$\boldsymbol{B}_{\text{eff}} = \boldsymbol{\nabla}\times\boldsymbol{A}_{\text{eff}}. \tag{1.35}$$

Similar equations with the subscript 'eff' replaced by 'ext' relate the external potentials to the external fields. Eq. (1.30) is gauge invariant and this invariance has been exploited in other

implementations of TDCDFT. [3] Note that Eq. (1.32) contains a functional derivative of the exchange correlation functional with respect to the current density so any approximate exchange-correlation potential should, in principle, depend on both particle and current density. Such an exchange-correlation potential has been proposed by Vignale and Kohn [15] and shown to yield improved results for the optical absorption spectrum of several semiconductors. [16]

1.3 Polarization and Current Density

Of the many results derived in Secs. 1.1 and 1.2, we emphasize several key formulas that are needed for computing the response of periodic materials to electromagnetic fields. Eqs. (1.6) and (1.9) define the macroscopic polarization in terms of the total internal electric field of the material and the internal current density respectively. Both of these quantities are available in TDCDFT: the total internal electric field is E_{eff} in Eq. (1.34) and the internal current density is $\boldsymbol{j}$ in Eq. (1.31), where one must remember to multiply this current density by the charge of an electron e for use in Maxwell's equations. Thus with TDCDFT we know all of the quantities in Eq. (1.6) except for the macroscopic susceptibility χ, which is in fact the response function of the material that we are seeking. Actually computing the quantities listed above is the subject of the remainder of this thesis.

We mention in passing that one of the main alternatives to using TDCDFT in the calculation of optical properties of periodic solids is the GW approximation. The GW approximation is a many-body perturbation theory based on DFT that produces absorption spectra that are very accurate. However, the GW approximation is also a very costly computation in comparison to TDCDFT [2, Pg. 1] and performs poorly on systems with strong correlations [17] since it is also based on DFT.

Chapter 2

Method

This chapter describes our real-space implementation of time-dependent current density functional theory (TDCDFT) for application to nonmetallic solids. We make use of the *ab initio* density functional theory FIREBALL program and describe the necessary modifications needed to support TDCDFT calculations. We show how to construct the effective scalar and vector potentials of Eqs. (1.32) and (1.33) and describe the use of the Coulomb gauge in constructing the classical electromagnetic contributions to these potentials. These scalar and vector potentials are included self-consistently in the time-dependent Kohn-Sham equation shown in Eq. (1.27). We end this chapter by listing the step-by-step process used to complete the TDCDFT computation.

2.1 FIREBALL

We choose to implement TDCDFT in the FIREBALL DFT program. FIREBALL is an *ab-initio* local-orbital density functional theory program with a nonlocal pseudopotential scheme. It is capable of performing molecular dynamics on large systems containing hundreds of atoms. (See Ref. [18] for an example of simulating a 644-atom deoxyribonucleic acid double-helix

poly(dG)·poly(dC) segment.) FIREBALL is also capable of performing optical frequency TDDFT calculations for finite systems [19] and this further reduces our efforts in adding support for TDCDFT calculations of periodic systems.

There are several features unique to FIREBALL that affect our implementation of TDCDFT. The energy functional in FIREBALL is not the typical Kohn-Sham energy functional from Eq. (1.23) but is rather based on a Harris-Foulkes functional that is modified to produce a self-consistent scheme called DOGS as described in Ref. [20]. FIREBALL computes the forces on the atoms using this energy functional in combination with the Hellman-Feynmann Theorem. These forces are then used to predict the motion of the atoms. [21, Pg. 3990] (This method is an alternative to solving the Schrödinger-like equation for the nuclei given in Eq. (1.17).)

The localized orbitals used in FIREBALL are slightly excited pseudoatomic orbitals confined to have a finite cutoff radius. The confinement of these orbitals makes this a tight-binding method and greatly reduces the number of interactions between orbitals. Several FIREBALL orbitals are shown in Fig. 2.1 to illustrate this confinement. For a comparison of orbitals in FIREBALL with other types of localized orbitals see Ref. [11, Ch. 15]. The numerical construction of these orbitals and the determination of the cutoff radius are described in Ref. [21, Sec. C]. A linear combination of these orbitals is used to form the independent-electron wave functions seen in Eq. (1.25). In Sec. 2.3, we compute the integrals of these orbitals with the gradient operator to construct the momentum and current density for use in TDCDFT.

In performing TDDFT and TDCDFT calculations in FIREBALL we first compute the ground-state electronic structure using the DOGS self-consistent scheme mentioned above. After this ground-state structure is found we proceed by fixing the positions of the nuclei in space, applying an external field, and propagating the particle density ρ in time as explained in Sec. 2.2. The LDA as parametrized by Ceperly and Alder [22] is used for the exchange

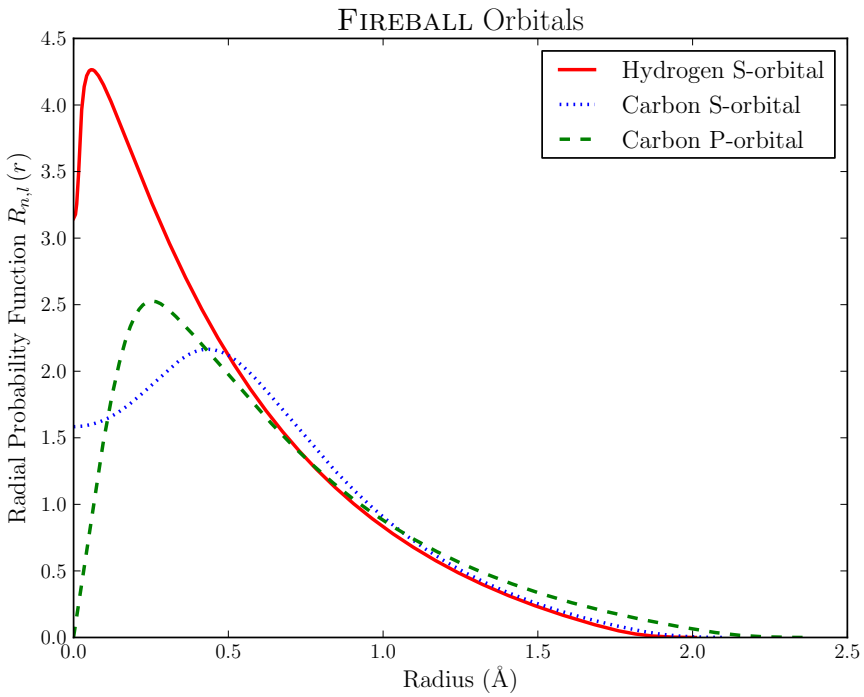

Figure 2.1 Several FIREBALL radial wave functions with finite cutoffs.

correlation functional in both the ground-state and excited-state calculations.

2.2 Time Dependent Current Density Functional Theory

We begin the description of our TDCDFT implementation within FIREBALL with a discussion of potentials and gauge transformations. It is instructive to rewrite Eq. (1.32) as

$$\boldsymbol{A}_{\text{eff}}(\boldsymbol{r},t) = \boldsymbol{A}_{\text{ext}}(\boldsymbol{r},t) + \boldsymbol{A}_{\text{EM}}(\boldsymbol{r},t) + \boldsymbol{A}_{\text{xc}}(\boldsymbol{r},t) \tag{2.1}$$

and Eq. (1.33) as

$$V_{\text{eff}}(\boldsymbol{r},t) = V_{\text{en}}(\boldsymbol{r}) - eV_{\text{ext}}(\boldsymbol{r},t) + V_{\text{EM}} + V_{\text{xc}} + \frac{e^2}{2m_e}\left(\boldsymbol{A}_{\text{eff}}^2 - \boldsymbol{A}_{\text{ext}}^2\right), \tag{2.2}$$

where A_{EM}, A_{xc}, V_{EM}, and V_{xc} are the electromagnetic vector potential, the exchange-correlation vector potential, the electromagnetic scalar potential, and the exchange-correlation scalar potential respectively. As explained in Sec. 1.2.4, Eq. (1.30) is gauge invariant so we are free to add the gradient of some scalar function Λ to any of the vector potentials in Eq. (2.1) as seen in the equation

$$\boldsymbol{A} \rightarrow \boldsymbol{A}' = \boldsymbol{A} + \boldsymbol{\nabla}\Lambda, \tag{2.3}$$

provided that there is also a change in the scalar potential of the form [4, Pg. 240]

$$V \rightarrow V' = V - \frac{\partial \Lambda}{\partial t}. \tag{2.4}$$

We choose to work in the Coulomb gauge for the electromagnetic (EM) potentials in Eqs. (2.1) and (2.2) so that $\boldsymbol{\nabla}\cdot\boldsymbol{A}_{\text{EM}} = 0$. These potentials then take the form: [4, Pgs. 241-2]

$$V_{\text{EM}}(\boldsymbol{x},t) = \frac{1}{4\pi\epsilon_0}\int d^3x' \, \frac{\rho(\boldsymbol{x}',t)}{|\boldsymbol{x}-\boldsymbol{x}'|} \text{ and} \tag{2.5}$$

$$\boldsymbol{A}_{\text{EM}}(\boldsymbol{x},t) = \frac{\mu_0}{4\pi}\int d^3x' \, \frac{1}{|\boldsymbol{x}-\boldsymbol{x}'|}\boldsymbol{j}_t\left(\boldsymbol{x}', t - \frac{|\boldsymbol{x}-\boldsymbol{x}'|}{c}\right), \tag{2.6}$$

where

$$\boldsymbol{j}_t = \boldsymbol{j} - \frac{1}{\mu_0 c^2} \boldsymbol{\nabla} \frac{\partial}{\partial t} V_{\text{eff}} \tag{2.7}$$

is the transverse current. The advantage of working in the Coulomb gauge here is that V_{EM} is instantaneous and is the same electrostatic term present in ground-state DFT. The disadvantage is that we must work with the retarded current density in solving for the effective vector potential, which involves the gradient of the effective potential V_{eff} as seen in Eq. (2.7). Notice also that this term depends on the retarded time and therefore contains some memory effects in addition to the memory effects included in the exchange-correlation potentials. [2, Pg.3]

As explained in Sec. 2.1, the ground-state particle density of our solid is first computed using DFT and then the charge and current densities must be found self consistently since the effective vector and scalar potentials depend on the particle and current densities. We choose to only include linear terms in Eqs. (2.1) and (2.2) and work within the ALDA as described in Sec. 1.2.4. We also ignore the current dependence of the exchange-correlation potential so that $\boldsymbol{A}_{\text{xc}} = 0$. The particle density is then propagated in time according to the equation

$$i\hbar \frac{\partial \rho}{\partial t} = \left[H\left(t\right), \rho \right] \tag{2.8}$$

by using a unitary Crank-Nicolson propagator as described in Ref. [19]. The expectation value of any operator A can be found using the equation [9, Pg. 363]

$$\langle A \rangle = \text{trace}\left(A\rho\right). \tag{2.9}$$

We use this equation at each time step to find and store the expectation values of the current density $\boldsymbol{j}$ and the macroscopic electric field E_{eff}. Using the current density (and multiplying by the electric charge e) we compute and store the polarization at each time step using Eq. (1.6).

In order to find the susceptibility and dielectric function of our solid, we proceed by taking the Fourier transform of the macroscopic electric field $\boldsymbol{E}_{\text{eff}}$ and the macroscopic polarization $\boldsymbol{P}$. Depending on the symmetry of the solid being studied, we may need to run the entire simulation up to three times with different external electric fields pointing in linearly-independent directions. By indicating the run number as a superscript we have the following three equations for the x-component of the macroscopic polarization:

$$\begin{aligned} P_1^{(1)}(\boldsymbol{r},\omega) &= \chi_{11}E_1^{(1)}(\omega) + \chi_{12}E_2^{(1)}(\omega) + \chi_{13}E_3^{(1)}(\omega) \\ P_1^{(2)}(\boldsymbol{r},\omega) &= \chi_{11}E_1^{(2)}(\omega) + \chi_{12}E_2^{(2)}(\omega) + \chi_{13}E_3^{(2)}(\omega) \\ P_1^{(3)}(\boldsymbol{r},\omega) &= \chi_{11}E_1^{(3)}(\omega) + \chi_{12}E_2^{(3)}(\omega) + \chi_{13}E_3^{(3)}(\omega) \end{aligned} \tag{2.10}$$

These equations can be written in matrix form and solved for χ_{11}, χ_{12}, and χ_{13}. Similar equations arise for the P_2 and P_3 components which can also be solved to give us χ_{21}, χ_{22}, χ_{23}, χ_{31}, χ_{32}, and χ_{33}. The resulting susceptibility tensor should be symmetric due to energy arguments but could contain off-diagonal elements depending on the symmetry of the solid. [6, Ch. 9]

2.3 Molecular Integrals

As explained in Sec. 2.2, our implementation of TDCDFT requires integrals of the basis orbitals with the gradient operator of the form

$$\langle \phi_1(\boldsymbol{r}-\boldsymbol{R}_1)\,|\boldsymbol{\nabla}|\,\phi_2(\boldsymbol{r}-\boldsymbol{R}_2)\rangle = \int d\boldsymbol{r}\,\phi_1(\boldsymbol{r}-\boldsymbol{R}_1)\,\boldsymbol{\nabla}\phi_2(\boldsymbol{r}-\boldsymbol{R}_2) \tag{2.11}$$

where ϕ_1 and ϕ_2 are any two basis orbitals located at $\boldsymbol{R}_1$ and $\boldsymbol{R}_2$ respectively. In this section we give a derivation of these integrals valid for a wide range of orbitals as described below. Due to the generality of the derivation we also give expressions for the kinetic energy, overlap, and dipole interactions.

We choose to work with orbitals of the form

$$\phi_i(\boldsymbol{r}) = R_{n_i,l_i}(r)\, S_{l_i,m_i}(\hat{\boldsymbol{r}}) \tag{2.12}$$

where $R_{n,l}$ is a numerical or analytical radial function, $S_{l,m}$ is a real spherical harmonic, r is the radial coordinate, and $\hat{\boldsymbol{r}}$ stands for the angular coordinates (θ, ϕ). (See Fig. 2.1 for some examples of numerical radial functions.) We use the following definition of the real spherical harmonics as given in Ref. [23]:[1]

$$S_{l,m} = \sqrt{\frac{2l+1}{4\pi}\frac{(l-|m|)!}{(l+|m|)!}} \cdot \begin{cases} \sqrt{2} P_l^m(\cos\theta)\cos(m\phi), & m > 0 \\ P_l^0(\cos\theta), & m = 0 \\ \sqrt{2} P_l^{|m|}(\cos\theta)\sin(|m|\,\phi), & m < 0 \end{cases}, \tag{2.13}$$

where P_l^m is an associated Legendre polynomial

$$P_l^m(x) = \frac{1}{2^l l!}\left(1-x^2\right)^{m/2}\frac{d^{l+m}}{dx^{l+m}}\left(x^2-1\right)^l. \tag{2.14}$$

(See Tab. 2.1 for the first few real spherical harmonics resulting from this definition.) Orbitals with different real spherical harmonics are often given abbreviated names based on spectroscopic notation (S, P, D, F, ...) [24, Pg. 303] and their Cartesian coordinate representation. For example, orbitals with the $S_{0,0}$, $S_{1,-1}$, $S_{1,0}$, and $S_{1,1}$ spherical harmonics are called s, p_y, p_z, and p_x orbitals respectively.

The real spherical harmonics have some important properties that we use in the following derivations of molecular integrals. In Ref. [25] it is shown that the real spherical harmonics form a complete orthonormal set such that

$$\int d\Omega\, S_{l,m}(\theta,\phi)\, S_{l',m'}(\theta,\phi) = \delta_{l,l'}\delta_{m,m'}. \tag{2.15}$$

[1] This definition of real spherical harmonics does not contain the Condon-Shortley factor present in most definitions of complex spherical harmonics.

$$
\begin{aligned}
S_{0,0} &= \sqrt{\frac{1}{4\pi}} && = \sqrt{\frac{1}{4\pi}} \\
S_{1,-1} &= \sqrt{\frac{3}{4\pi}} \sin(\theta) \sin(\phi) && = \sqrt{\frac{3}{4\pi}} \frac{y}{r} \\
S_{1,0} &= \sqrt{\frac{3}{4\pi}} \cos(\theta) && = \sqrt{\frac{3}{4\pi}} \frac{z}{r} \\
S_{1,1} &= \sqrt{\frac{3}{4\pi}} \sin(\theta) \cos(\phi) && = \sqrt{\frac{3}{4\pi}} \frac{x}{r} \\
S_{2,-2} &= \sqrt{\frac{15}{144\pi}} \left[3 - 3\cos^2(\theta)\right] \sin(2\phi) && = \sqrt{\frac{15}{4\pi}} \frac{xy}{r^2} \\
S_{2,-1} &= \sqrt{\frac{15}{4\pi}} \cos(\theta) \sin(\theta) \sin(\phi) && = \sqrt{\frac{15}{4\pi}} \frac{yz}{r^2} \\
S_{2,0} &= -\sqrt{\frac{5}{4\pi}} \left[\frac{1}{2} - \frac{3}{2}\cos^2(\theta)\right] && = \sqrt{\frac{5}{16\pi}} \frac{3z^2 - r^2}{r^2} \\
S_{2,1} &= \sqrt{\frac{15}{4\pi}} \cos(\phi) \cos(\theta) \sin(\theta) && = \sqrt{\frac{15}{4\pi}} \frac{xz}{r^2} \\
S_{2,2} &= \sqrt{\frac{15}{144\pi}} \left[3 - 3\cos^2(\theta)\right] \cos(2\phi) && = \sqrt{\frac{135}{144\pi}} \frac{x^2 - y^2}{r^2}
\end{aligned}
$$

Table 2.1 Real spherical harmonics for $l = 0, 1,$ and 2, where $r^2 = x^2 + y^2 + z^2$. Note that the above relations can be used to solve for the variables $x, y,$ and z: $y = r\sqrt{\frac{4\pi}{3}} S_{1,-1}$, $z = r\sqrt{\frac{4\pi}{3}} S_{1,0}$, and $x = r\sqrt{\frac{4\pi}{3}} S_{1,1}$.

The real spherical harmonics are also related to the the complex spherical harmonics via the formula

$$\sum_{m=-l}^{l} S_{l,m}\left(\hat{r}_1\right) S_{l,m}\left(\hat{r}_2\right) = \sum_{m=-l}^{l} Y_l^m\left(\hat{r}_1\right) Y_l^m\left(\hat{r}_2\right), \tag{2.16}$$

where the complex spherical harmonics Y_l^m are defined according to Ref. [25]. This property is important because it allows us to rewrite the Rayleigh Expansion of a plane wave in terms of real spherical harmonics: [9, Pg. 261]

$$\begin{aligned} e^{i\boldsymbol{k}\cdot\boldsymbol{r}} &= 4\pi \sum_{l=0}^{\infty} i^l j_l\left(kr\right) \sum_{m=-l}^{l} \left[Y_l^m\left(\hat{\boldsymbol{k}}\right)\right]^* Y_l^m\left(\hat{\boldsymbol{r}}\right) \\ &= 4\pi \sum_{l=0}^{\infty} i^l j_l\left(kr\right) \sum_{m=-l}^{l} S_{l,m}\left(\hat{\boldsymbol{k}}\right) S_{l,m}\left(\hat{\boldsymbol{r}}\right) \end{aligned}, \tag{2.17}$$

where j_l is a spherical Bessel function related to the regular Bessel functions J_l by the relation: [4, Pg. 426]

$$j_l\left(z\right) = \sqrt{\frac{\pi}{2z}} J_{l+1/2}\left(z\right). \tag{2.18}$$

Furthermore, a comparison of the real and imaginary parts of the left- and right-hand sides of Eq. (2.17) give us the following expansion for an incoming plane wave:

$$e^{-i\boldsymbol{k}\cdot\boldsymbol{r}} = 4\pi \sum_{l=0}^{\infty} \left(-i\right)^l j_l\left(kr\right) \sum_{m=-l}^{l} S_{l,m}\left(\hat{\boldsymbol{k}}\right) S_{l,m}\left(\hat{\boldsymbol{r}}\right). \tag{2.19}$$

Eq. (2.16) is also useful in expanding the Coulomb kernel for computing integrals of the type shown in Eq. (2.5):

$$\frac{1}{|\boldsymbol{r}_1 - \boldsymbol{r}_2|} = \sum_{l=-\infty}^{\infty} \frac{4\pi}{2l+1} \frac{r_<^l}{r_>^{l+1}} \sum_{m=-l}^{l} S_{l,m}\left(\hat{\boldsymbol{r}}_1\right) S_{l,m}\left(\hat{\boldsymbol{r}}_2\right), \tag{2.20}$$

where $r_<$ ($r_>$) is the smaller (larger) of $|\boldsymbol{r}_1|$ and $|\boldsymbol{r}_2|$.

Our derivations of molecular integrals eventually result in a sum of integrals over real spherical harmonics multiplied by radial Hankel transforms. The integrals over real spherical harmonics can all be performed analytically since the real spherical harmonics have the

following property: [25]

$$S_{l_1,m_1}(\hat{\boldsymbol{r}})\, S_{l_2,m_2}(\hat{\boldsymbol{r}}) = \sum_{l_3,m_3} \langle l_3 m_3 \,|l_1 m_1|\, l_2 m_2\rangle_R \; S_{l_3,m_3}(\hat{\boldsymbol{r}}), \tag{2.21}$$

where $\langle l_3 m_3 \,|l_1 m_1|\, l_2 m_2\rangle_R$ is a real Gaunt (R-Gaunt) coefficient that is zero unless $l_1 \in \{l_{max}, l_{max-2}, ..., l_{min}\}$, where $l_{max} = l_2 + l_3$,

$$l_{min} = \begin{cases} \kappa(l_2, l_3, m_2, m_3) & \text{if } \kappa(l_2, l_3, m_2, m_3) + l_{max} \text{ is even} \\ \kappa(l_2, l_3, m_2, m_3) + 1 & \text{if } \kappa(l_2, l_3, m_2, m_3) + l_{max} \text{ is odd} \end{cases},$$

and $\kappa(l_2, l_3, m_2, m_3) = \max(|l_2 - l_3|, \min(|m_2 + m_3|, |m_2 - m_3|))$. This property of the real spherical harmonics allows us to write any finite product of real spherical harmonics evaluated at the same angular coordinates as a finite sum of single real spherical harmonics evaluated at the same coordinates, or in symbols,

$$S_{l_1,m_1}(\hat{\boldsymbol{r}})\, S_{l_2,m_2}(\hat{\boldsymbol{r}}) \cdots S_{l_n,m_n}(\hat{\boldsymbol{r}}) = \sum_{l=0}^{l_{\max}} \sum_{m=-l}^{l} a_{l,m} S_{l,m}(\hat{\boldsymbol{r}}) \tag{2.22}$$

for some expansion coefficients $a_{l,m}$. In our computation we compute the R-Gaunt coefficients with the SymPy computer algebra system and store the results in a hash table (associated array). [26]

Our main mathematical tools for carrying out the derivations of molecular integrals are the Fourier and inverse Fourier transforms. We define the Fourier and inverse Fourier transforms in accordance with the definition in Ref. [9, Pg. 30]:

$$\overline{f}(\boldsymbol{k}) = \mathcal{F}\{f(\boldsymbol{x})\}(\boldsymbol{k}) \quad = (2\pi)^{-n/2} \int_{\mathbb{R}^n} d\boldsymbol{x}\, f(\boldsymbol{x})\, e^{-i\boldsymbol{k}\cdot\boldsymbol{x}} \tag{2.23}$$

$$f(\boldsymbol{r}) = \mathcal{F}^{-1}\left\{\overline{f}(\boldsymbol{k})\right\}(\boldsymbol{x}) = (2\pi)^{-n/2} \int_{\mathbb{R}^n} d\boldsymbol{k}\, \overline{f}(\boldsymbol{k})\, e^{i\boldsymbol{k}\cdot\boldsymbol{x}} \tag{2.24}$$

where n is a natural number ($n = 1, 2, 3, \ldots$). If the Fourier transforms exist for some functions f and g then the Cross-correlation Theorem holds: [27]

$$[f \star g](\boldsymbol{x}) = (2\pi)^{n/2}\, \mathcal{F}\left\{\overline{f}(\boldsymbol{k})\, \overline{g}^*(\boldsymbol{k})\right\}(\boldsymbol{x}), \tag{2.25}$$

where

$$[f \star g](\boldsymbol{x}) = \int_{\mathbb{R}^n} d\boldsymbol{x}_1 \, f(\boldsymbol{x}_1) \, g^*(\boldsymbol{x}_1 + \boldsymbol{x}) \tag{2.26}$$

and the $*$ symbol is used to denote complex conjugation. (See Sec. A.1 for a proof of the Cross-correlation Theorem.) We will use this theorem repeatedly in the following derivations. For the gradient integrals we need the following theorem for the Fourier transform of the derivative of a function: [28, Pg. 401]

$$\mathcal{F}\left\{\frac{\partial^j}{\partial x_i^j} f(\boldsymbol{x})\right\}(\boldsymbol{k}) = (ik_i)^j \, \mathcal{F}\{f(\boldsymbol{x})\}(\boldsymbol{k}) \tag{2.27}$$

$$\mathcal{F}^{-1}\left\{\frac{\partial^j}{\partial x_i^j} f(\boldsymbol{x})\right\}(\boldsymbol{k}) = (-ik_i)^j \, \mathcal{F}^{-1}\{f(\boldsymbol{x})\}(\boldsymbol{k}) \,. \tag{2.28}$$

The derivations of the molecular integrals are straightforward applications of the above theorems involving the real spherical harmonics and Fourier transforms. Due to the length and complexity of the formulas involved we refer the reader to App. A for the derivations and results. The derivations are valid for any point in space and thus avoid the need to use rotation matrices like the original FIREBALL integrals do. [21, Pg. 3986] Great care has been taken to write the radial integrals in such a way as to make use of the Logarithmic Fast Fourier Transform (FFTLog) in order to accelerate the numerical evaluation of the integrals. The FFTLog provides this acceleration because it uses two $\mathcal{O}(N \log N)$ FFTs. [29, App. B.4] This is to be contrasted with most other types of numerical integration that use $\mathcal{O}(N^2)$ algorithms since they have to sample at least N points for each of the N integrals computed on the grid. Some of the other advantages and limitations of this algorithm are described in Sec. 3.2.

2.4 Gradients of Potentials

When computing the electric fields and the transverse current in our implementation of TDCDFT we need to compute the gradient of scalar potentials of the form

$$\langle \phi_\alpha (\boldsymbol{r} - \boldsymbol{R}_1) \left| \boldsymbol{\nabla} V (\boldsymbol{r} - \boldsymbol{R}_3) \right| \phi_\beta (\boldsymbol{r} - \boldsymbol{R}_2) \rangle . \tag{2.29}$$

Since these gradients are not precomputed and stored in tables like most of FIREBALL's integrals, (see Sec. 2.3 for several examples), we compute them using a centered finite difference scheme of the form

$$\begin{aligned} \boldsymbol{\nabla} V (\boldsymbol{r} - \boldsymbol{R}_3) \approx & \frac{V (\boldsymbol{r} - \boldsymbol{R}_3 + h_x \hat{x}) - V (\boldsymbol{r} - \boldsymbol{R}_3 - h_x \hat{x})}{2h_x} \hat{x} \\ & + \frac{V (\boldsymbol{r} - \boldsymbol{R}_3 + h_y \hat{y}) - V (\boldsymbol{r} - \boldsymbol{R}_3 - h_y \hat{y})}{2h_y} \hat{y} \\ & + \frac{V (\boldsymbol{r} - \boldsymbol{R}_3 + h_z \hat{z}) - V (\boldsymbol{r} - \boldsymbol{R}_3 - h_z \hat{z})}{2h_z} \hat{z} \end{aligned} \tag{2.30}$$

where V is replaced with either V_{eff} for computing the macroscopic electric field $\boldsymbol{E}_{\text{eff}}$ in Eq. (1.34) or V_{EM} for computing the transverse current in Eq. (2.7).

Care must be taken when using the centered difference approximation in Eq. (2.30) for several reasons. Since the integrals in FIREBALL are stored in tables, their values must be interpolated for a given set of $\boldsymbol{R}_1$, $\boldsymbol{R}_2$, and $\boldsymbol{R}_3$ vectors. Thus the grid spacings h_x, h_y, and h_z cannot be smaller than the error tolerance of the interpolator. Furthermore, since we are shifting the location of the potential, integrals that were once one- and two-center integrals are now two- and three-center integrals as shown in Fig. 2.2. This complication requires a change in what tables are used to look up the values of the integrals used in the finite difference scheme.

2.5 Outline of Calculation and Approximations

The following list is a summary of our TDCDFT method:

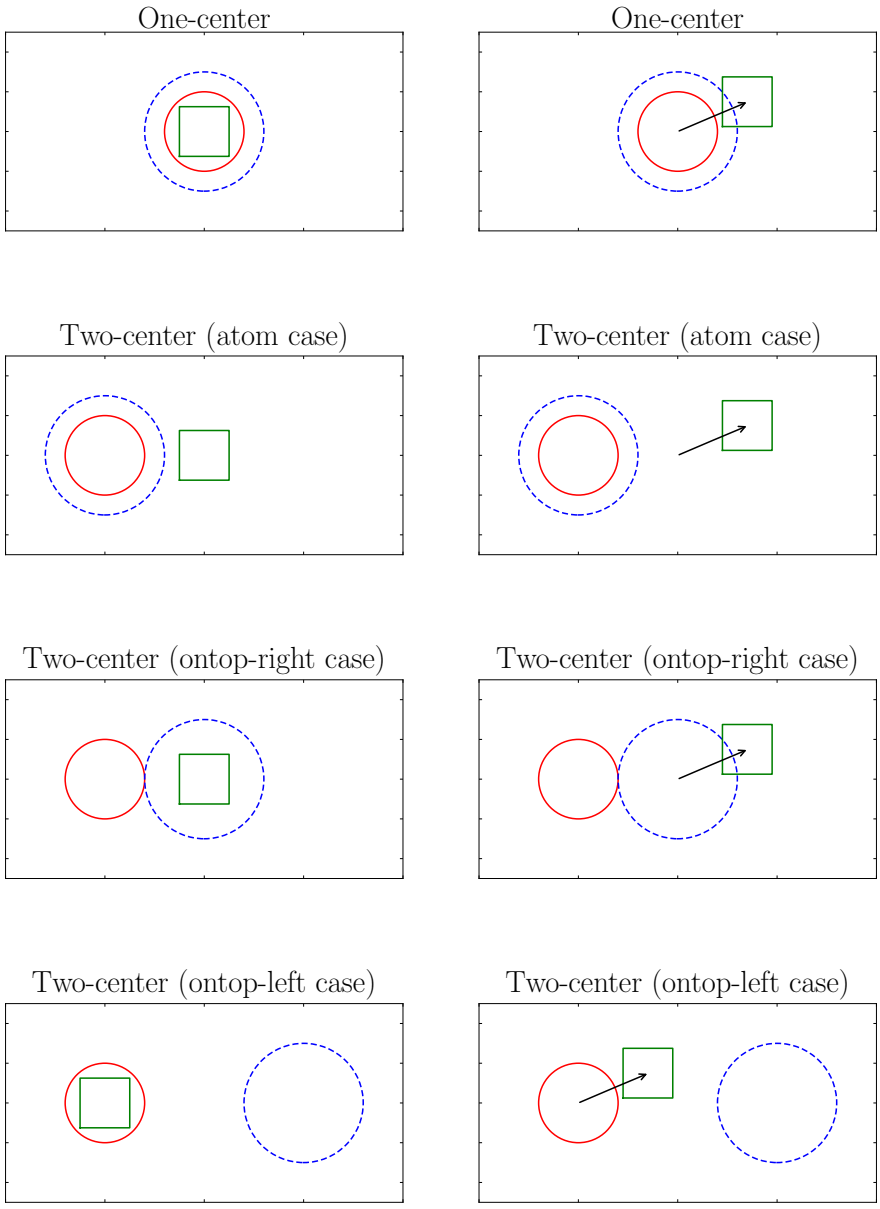

Figure 2.2 A representation of the one- and two-center integrals in FIREBALL before shifting (left column) and after shifting (right column). The square represents the location of the potential that is being shifted and the circles represent the locations of the orbitals. Notice that the one-center integral becomes a two-center integral, the ontop-right and ontop-left two-center integrals become three-center integrals, and the atom two-center integral remains a two-center integral.

1. The ground state density ρ is obtained by relaxing the solid using DFT.

2. Precompute the gradient integrals as explained in Sec. 2.3

3. Perform one to three runs with the initial E-field pointing in linearly independent directions, depending on the symmetry of the solid.

   (a) An electric field is applied to the system as a delta function at time $t = 0$. (This field can be included in either the external vector or scalar potential.)

   (b) Propagate the density in time using a Crank-Nicholson propagator.

   (c) E_{mac} and P_{mac} are computed and stored at each time step.

   (d) Fourier transform both E_{mac} and P in time.

4. Solve for the electric susceptibility using a linear solve if necessary. (See Sec. 2.2 for details on the linear solve.)

We also list here several of the key approximations made in implementing our TDCDFT method:

1. Neglect electric quadrupole and higher terms (Eq. (1.2))

2. Born-Oppenheimer approximation (Sec. 1.2.2)

3. "N-representable" density (Sec. 1.2.3)

4. Kohn-Sham ansatz (Sec. 1.2.3)

5. Linear response, LDA, ALDA (Sec. 2.2)

Chapter 3

Results

Plots of several gradient and kinetic energy integrals are displayed for Gaussian-type Orbitals (GTOs) using both the computation described in Sec. 2.3 and the analytical solutions. We also plot several of these integrals using FIREBALL orbitals for comparison. A brief summary of the results and our method is given.

3.1 Gradient and Kinetic Energy Plots

We compute the gradient and kinetic energy integrals at 256 logarithmically-spaced radial grid points r from 1×10^{-5} to 1×10^{4} Å using the derivations of Sec. 2.3. We also compute these integrals with $r = 0$ using the composite Simpsons rule for a total of 129 points. The error in the 2-norm for the logarithmically-spaced integrals is displayed in the legend of each figure. We compute all of the integrals with a displacement vector of $\boldsymbol{R}_{21} = \boldsymbol{R}_2 - \boldsymbol{R}_1 = (r, \theta = \pi/5, \phi = \pi/7)$, where $\boldsymbol{R}_1$ is the location of the left orbital, $\boldsymbol{R}_2$ is the location of the right orbital, and r varies logarithmically as described above. The GTOs are of the form given in Sec. 2.3 with the radial functions given by $N_\alpha \exp(-\alpha r^2)$, where N_α is a normalization factor. We set $\alpha = 4$ for the left orbital and $\alpha = 5$ for the right orbital.

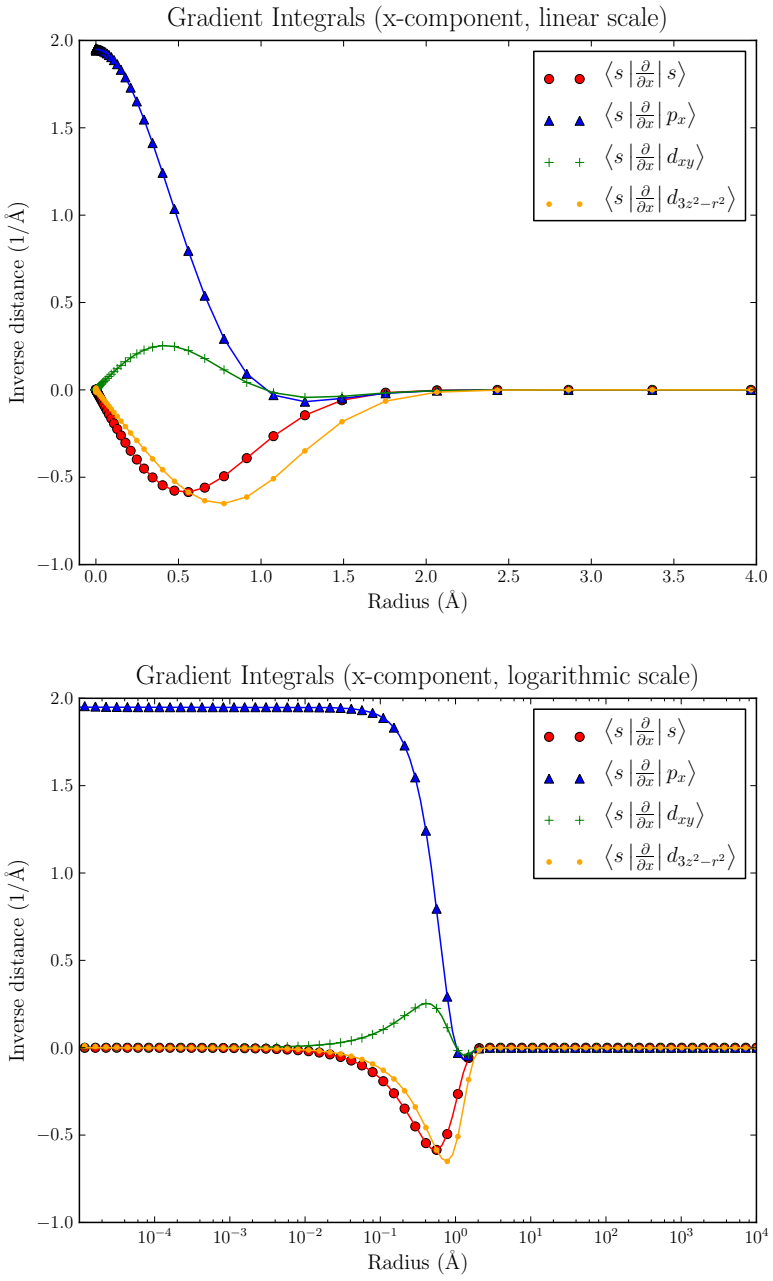

Figure 3.1 The x-component of the gradient integrals using Gaussian-type orbitals and the derivation in Sec. 2.3. The analytical solutions are plotted using solid lines for comparison.

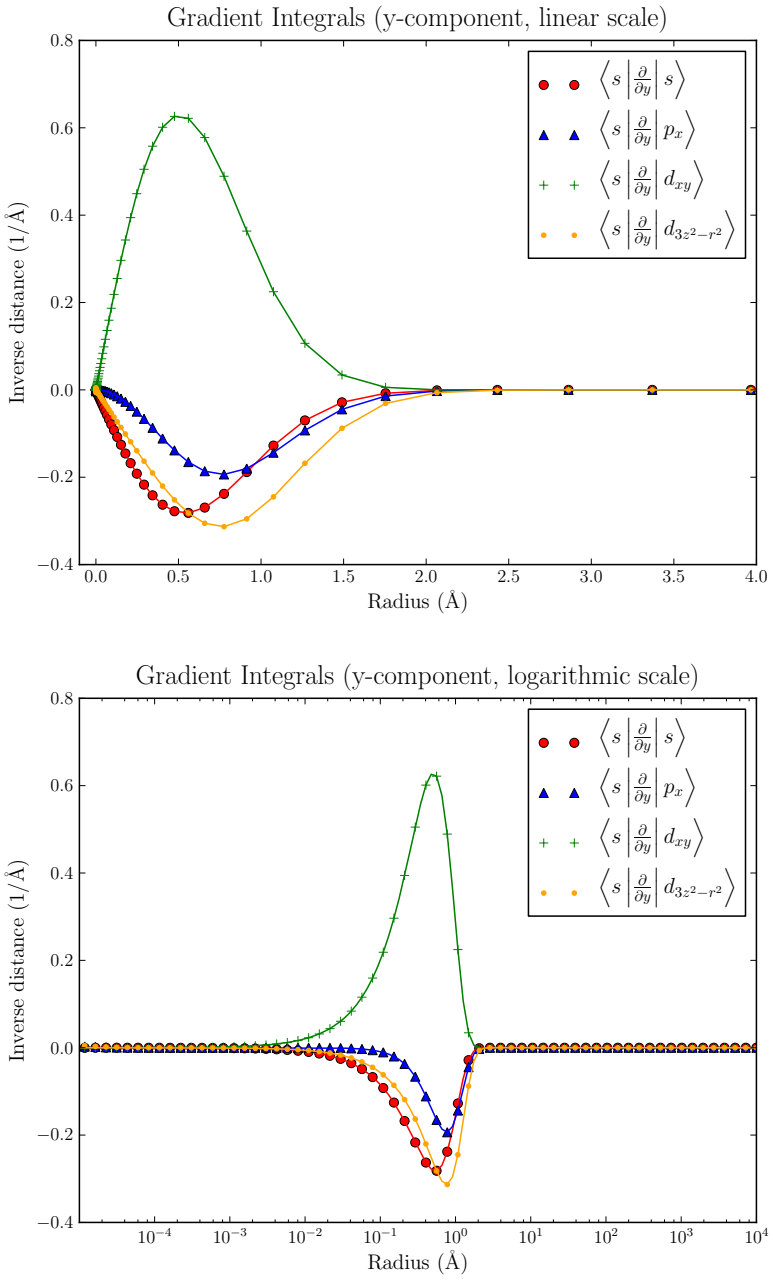

Figure 3.2 The y-component of the gradient integrals using Gaussian-type orbitals and the derivation in Sec. 2.3. The analytical solutions are plotted using solid lines for comparison.

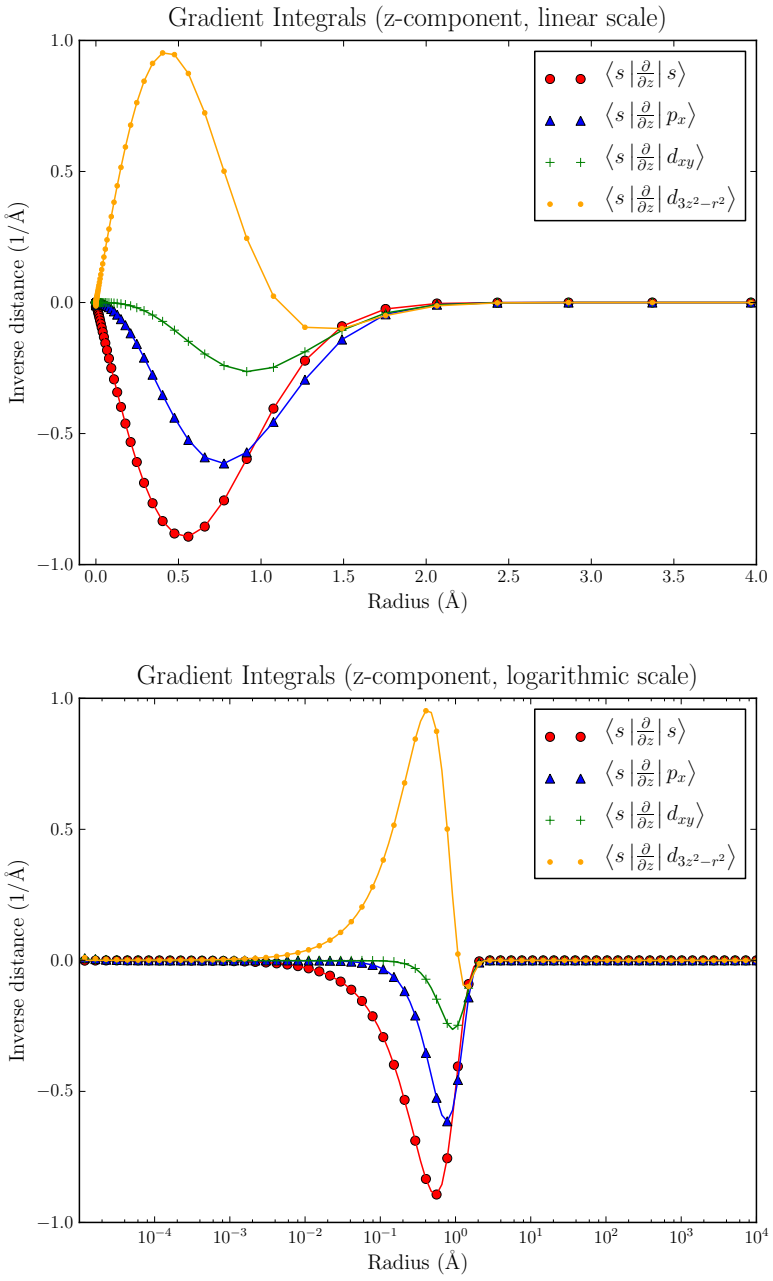

Figure 3.3 The z-component of the gradient integrals using Gaussian-type orbitals and the derivation in Sec. 2.3. The analytical solutions are plotted using solid lines for comparison.

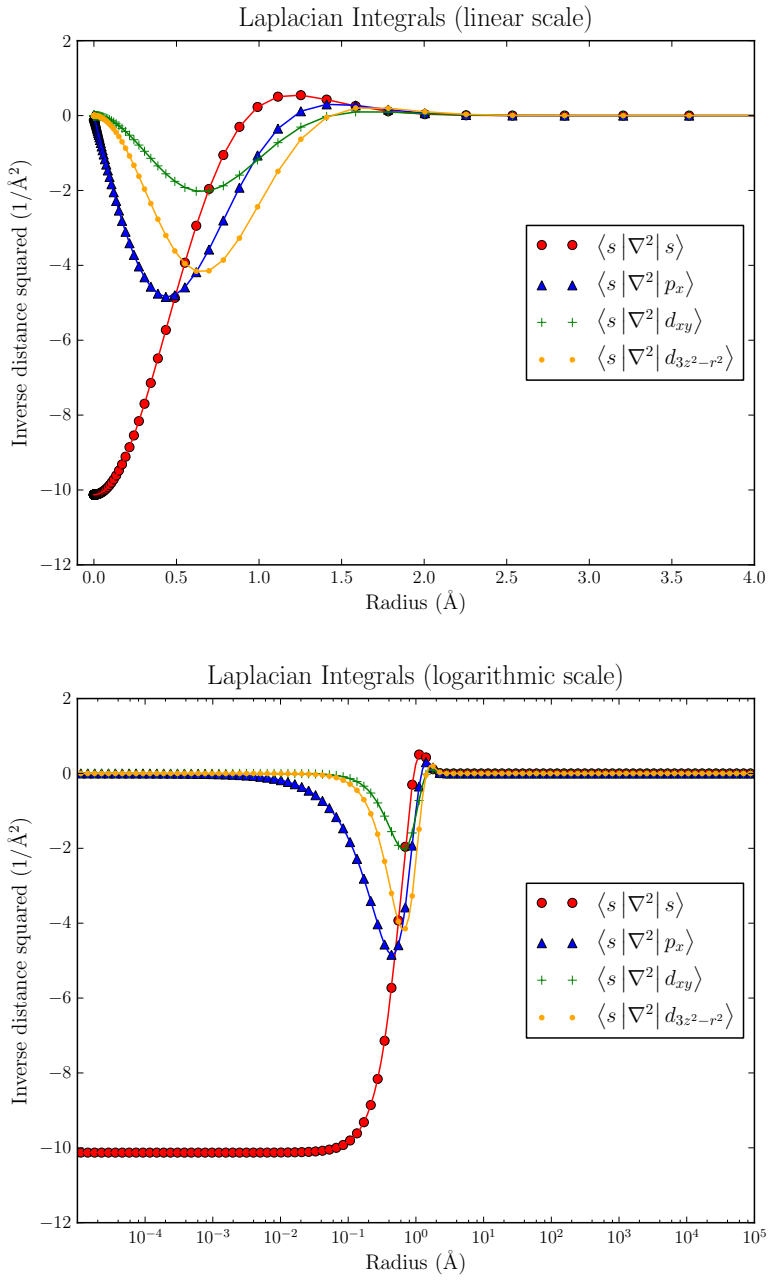

Figure 3.4 The Laplacian integrals using Gaussian-type orbitals and the derivation in Sec. 2.3. The analytical solutions are plotted using solid lines for comparison.

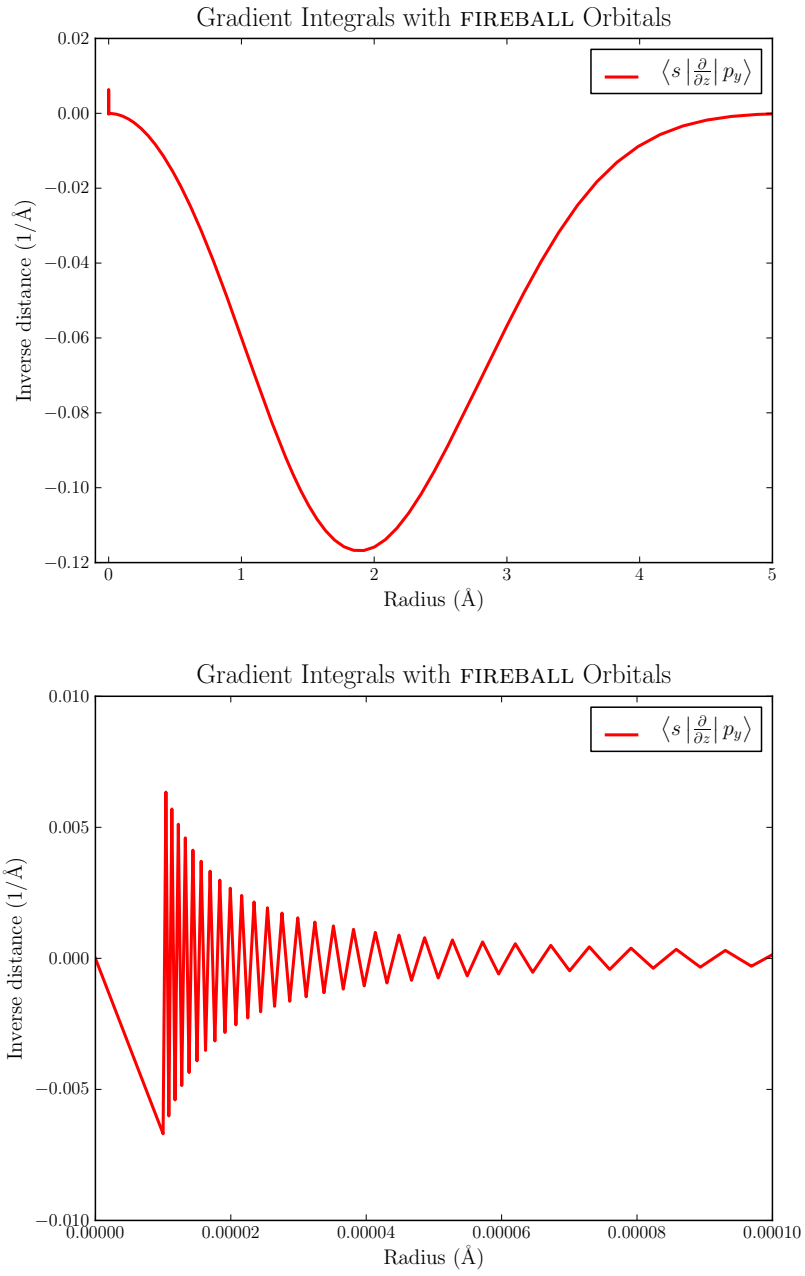

Figure 3.5 The z-component of the gradient integrals using FIREBALL orbitals and the derivation in Sec. 2.3. Notice the ringing present near the origin as shown clearly in the extremely zoomed axes of the second plot.

The plots in this section show excellent agreement between our numerical integrals and the analytical solutions for the gradient and kinetic energy integrals with GTOs. The error in the 2-norm for the logarithmically spaced gradient integrals with 1025 points is below 1×10^{-8} 1/Å for all of the interactions between s, p, and d orbitals except for those that are nonzero near the origin which have errors below 1×10^{-4}. The reason that there is increased error near the origin is that we must divide by the radius in the final step of the algorithm and dividing by small numbers increases the error. The FFTLog algorithm used here is particularly well-suited for these integrals because it samples the functions on a logarithmically-spaced grid and the functions being sampled vary most rapidly at the origin while being very smooth far away from the origin. However, as seen in Fig. 3.5, this algorithm suffers from a condition known as ringing, which is brought on by a response to sudden steps such as the finite cutoff in our FIREBALL orbitals. Because the ringing appears just near the origin, a simple fix exists of computing several integrals near the origin with a different algorithm and interpolating between them as described in Ref. [30, Pg. 3]. The FFTLog algorithm also suffers from aliasing since it is based on the Fast Fourier Transform (FFT) algorithm but this is easily resolved in our calculations by removing the aliased points.

3.2 Conclusion

We have outlined a real-space time-domain TDCDFT method for calculating the optical response of periodic systems. This method requires the computation of the gradient molecular integrals for forming the electric current density and the vector potential. A derivation of these integrals is given in Sec. 2.3 and several of them are shown in Sec. 3.1. Because of the generality of the derivation, we have also derived the kinetic energy, dipole, and overlap molecular integrals. The efficient evaluation of these integrals using the aforementioned derivations relies on the rapid evaluation of the Hankel transform, which is provided by our

implementation of the FFTLog.

As we are still in the testing phase of our simulations, we do not present any dielectric functions in this thesis. However, with the computation of the momentum integrals shown in Sec. 3.1 and the gradient of the potentials described in Sec. 2.4 we have most of the key components of our TDCDFT computation completed and well-tested. The method we present in Ch. 2 is very general and can be applied to solids without any particular symmetry as opposed to previous implementations of TDCDFT. [3] Furthermore, it is straightforward to extend the computation to the nonlinear regime by not ignoring the nonlinear terms in Eqs. (2.1) and (2.2). It also has an advantage over implementations purely in the frequency domain since we have spatial information about charge and current densities in the solid.

Bibliography

[1] S. K. Ghosh and A. K. Dhara, "Density-functional theory of many-electron systems subjected to time-dependent electric and magnetic fields," Phys. Rev. A **38,** 1149–1158 (1988).

[2] N. T. Maitra, I. Souza, and K. Burke, "Current-density functional theory of the response of solids," Phys. Rev. B **68,** 045109 (2003).

[3] F. Kootstra, P. L. de Boeij, and J. G. Snijders, "Application of time-dependent density-functional theory to the dielectric function of various nonmetallic crystals," Phys. Rev. B **62,** 7071–7083 (2000).

[4] J. D. Jackson, *Classical Electrodynamics*, 3 ed. (John Wiley & Sons, 1999).

[5] F. N. H. Robinson, *Macroscopic Electromagnetism* (Pergamon Press, New York, 1973).

[6] R. E. Newnham, *Properties of materials : anisotropy, symmetry, structure* (Oxford University Press, New York, 2005).

[7] H. T. Stokes, *Solid State Physics*, 4 ed. (Brigham Young University, 2007).

[8] J. Thijssen, *Computational Physics* (Cambridge University Press, New York, 2007).

[9] E. Merzbacher, *Quantum Mechanics*, 3rd ed. (John Wiley & Sons, 1998).

[10] A. Raab, "On the Dirac-Frenkel/McLachlan variational principle," Chemical Physics Letters **319,** 674–678 (2000).

[11] R. M. Martin, *Electronic structure: basic theory and practical methods* (Cambridge University Press, 2004).

[12] P. Hohenberg and W. Kohn, "Inhomogeneous Electron Gas," Phys. Rev. **136,** B864–B871 (1964).

[13] W. Kohn and L. J. Sham, "Self-Consistent Equations Including Exchange and Correlation Effects," Phys. Rev. **140,** A1133–A1138 (1965).

[14] E. Runge and E. K. U. Gross, "Density-Functional Theory for Time-Dependent Systems," Phys. Rev. Lett. **52,** 997 (1984).

[15] G. Vignale and W. Kohn, "Current-Dependent Exchange-Correlation Potential for Dynamical Linear Response Theory," Phys. Rev. Lett. **77,** 2037–2040 (1996).

[16] P. L. de Boeij, F. Kootstra, J. A. Berger, R. van Leeuwen, and J. G. Snijders, "Current density functional theory for optical spectra: A polarization functional," The Journal of Chemical Physics **115,** 1995–1999 (2001).

[17] C. Friedrich and A. S. and, "Many-Body Perturbation Theory: The GW Approximation," Computational Nanoscience: Do It Yourself! (2010).

[18] J. P. Lewis, P. Ordejón, and O. F. Sankey, "Electronic-structure-based molecular-dynamics method for large biological systems: Application to the 10 basepair poly(dG)·poly(dC) DNA double helix," Phys. Rev. B **55,** 6880–6887 (1997).

[19] B. C. Hess, D. S. Jensen, and I. Okhrimenko, "Spatial distribution of electron densities during optical excitation of C60," Phys. Rev. B (submitted) (2010).

[20] A. A. Demkov, J. Ortega, O. F. Sankey, and M. P. Grumbach, "Electronic structure approach for complex silicas," Phys. Rev. B **52,** 1618–1630 (1995).

[21] O. F. Sankey and D. J. Niklewski, "Ab initio multicenter tight-binding model for molecular-dynamics simulations and other applications in covalent systems," Phys. Rev. B **40,** 3979–3995 (1989).

[22] D. M. Ceperley and B. J. Alder, "Ground State of the Electron Gas by a Stochastic Method," Phys. Rev. Lett. **45,** 566–569 (1980).

[23] M. A. Blanco, M. Flórez, and M. Bermejo, "Evaluation of the rotation matrices in the basis of real spherical harmonics," Journal of Molecular Structure: THEOCHEM **419,** 19–27 (1997).

[24] P. A. Tipler and R. A. Llewellyn, *Modern Physics*, 4 ed. (W. H. Freeman and Company, New York, 2003).

[25] H. H. H. Homeier and E. O. Steinborn, "Some properties of the coupling coefficients of real spherical harmonics and their relation to Gaunt coefficients," Journal of Molecular Structure: THEOCHEM **368,** 31–37 (1996), proceedings of the Second Electronic Computational Chemistry Conference.

[26] SymPy Development Team, *SymPy: Python library for symbolic mathematics*, 2010.

[27] E. W. Weisstein, "Cross-Correlation Theorem,", MathWorld–A Wolfram Web Resource, 2010.

[28] N. H. Asmar, *Partial Differential Equations with Fourier series and boundary value problems*, 2 ed. (Pearson Prentice Hall, New Jersey, 2005).

[29] A. J. S. Hamilton, "Uncorrelated modes of the non-linear power spectrum," Monthly Notices of the Royal Astronomical Society **312,** 257–284 (2000).

[30] M. Toyoda and T. Ozaki, "Numerical evaluation of electron repulsion integrals for pseudoatomic orbitals and their derivatives," The Journal of Chemical Physics **130,** 124114 (2009).

Appendix A

Derivations

A.1 Cross-correlation Theorem

$$
\begin{aligned}
&\mathcal{F}\left\{\overline{f}\left(\boldsymbol{k}\right)\overline{g}^{*}\left(\boldsymbol{k}\right)\right\}\left(\boldsymbol{x}\right)\\
&=\left(2\pi\right)^{-n/2}\int_{\mathbb{R}^{n}}d\boldsymbol{k}\overline{f}\left(\boldsymbol{k}\right)\overline{g}^{*}\left(\boldsymbol{k}\right)e^{-i\boldsymbol{k}\cdot\boldsymbol{x}}\\
&=\left(2\pi\right)^{-n/2}\int_{\mathbb{R}^{n}}d\boldsymbol{k}\left[\left(2\pi\right)^{-n/2}\int_{\mathbb{R}^{n}}d\boldsymbol{x}_{1}\,f\left(\boldsymbol{x}_{1}\right)e^{-i\boldsymbol{k}\cdot\boldsymbol{x}_{1}}\right]\left[\left(2\pi\right)^{-n/2}\int_{\mathbb{R}^{n}}d\boldsymbol{x}_{2}\,g\left(\boldsymbol{x}_{2}\right)e^{-i\boldsymbol{k}\cdot\boldsymbol{x}_{2}}\right]^{*}e^{-i\boldsymbol{k}\cdot\boldsymbol{x}}\\
&=\left(2\pi\right)^{-n/2}\int_{\mathbb{R}^{n}}d\boldsymbol{x}_{1}\,f\left(\boldsymbol{x}_{1}\right)\int_{\mathbb{R}^{n}}d\boldsymbol{x}_{2}\,g^{*}\left(\boldsymbol{x}_{2}\right)\left(2\pi\right)^{-n}\int_{\mathbb{R}^{n}}d\boldsymbol{k}e^{i\boldsymbol{k}\cdot\left[\boldsymbol{x}_{2}-\left(\boldsymbol{x}_{1}+\boldsymbol{x}\right)\right]}\\
&=\left(2\pi\right)^{-n/2}\int_{\mathbb{R}^{n}}d\boldsymbol{x}_{1}\,f\left(\boldsymbol{x}_{1}\right)\int_{\mathbb{R}^{n}}d\boldsymbol{x}_{2}\,g^{*}\left(\boldsymbol{x}_{2}\right)\delta\left[\boldsymbol{x}_{2}-\left(\boldsymbol{x}_{1}+\boldsymbol{x}\right)\right]\\
&=\left(2\pi\right)^{-n/2}\int_{\mathbb{R}^{n}}d\boldsymbol{x}_{1}\,f\left(\boldsymbol{x}_{1}\right)g^{*}\left(\boldsymbol{x}_{1}+\boldsymbol{x}\right)\\
&=\left(2\pi\right)^{-n/2}\left[f\star g\right]\left(\boldsymbol{x}\right)
\end{aligned}
\tag{A.1}
$$

In this proof we have used the definition of the dirac delta function given in Ref. [9, Pg. 634].

A.2 Fourier Transform of Orbitals

First we derive the very general case of the Fourier transform of an orbital multiplied by a radial monomial and a real spherical harmonic:

$$
\begin{aligned}
&\mathcal{F}\left\{\phi_1\left(\boldsymbol{r}\right) r^{n_2} S_{l_2,m_2}\left(\hat{\boldsymbol{r}}\right)\right\}\left(\boldsymbol{k}\right) \\
&= \left(2\pi\right)^{-3/2} \int_{\mathbb{R}^3} d\boldsymbol{r}\, R_{n_1,l_1}\left(r\right) S_{l_1,m_1}\left(\hat{\boldsymbol{r}}\right) r^{n_2} S_{l_2,m_2}\left(\hat{\boldsymbol{r}}\right) e^{-i\boldsymbol{k}\cdot\boldsymbol{r}} \\
&= \left(2\pi\right)^{-3/2} \int_{\mathbb{R}^3} d\boldsymbol{r}\, R_{n_1,l_1}\left(r\right) S_{l_1,m_1}\left(\hat{\boldsymbol{r}}\right) r^{n_2} S_{l_2,m_2}\left(\hat{\boldsymbol{r}}\right) \\
&\qquad \left[4\pi \sum_{l=0}^{\infty} \left(-i\right)^l \sqrt{\frac{\pi}{2kr}} J_{l+1/2}\left(kr\right) \sum_{m=-l}^{l} S_{l,m}\left(\hat{\boldsymbol{k}}\right) S_{l,m}\left(\hat{\boldsymbol{r}}\right)\right] \\
&= \left(2\pi\right)^{-3/2} \left(4\pi\right) \left(\frac{\pi}{2}\right)^{-1/2} \sum_{l=0}^{\infty} \sum_{m=-l}^{l} \left(-i\right)^l S_{l,m}\left(\hat{\boldsymbol{k}}\right) \\
&\qquad \int r^2 dr\, R_{n_1,l_1}\left(r\right) r^{n_2} \left(kr\right)^{-1/2} J_{l+1/2}\left(kr\right) \int d\Omega\, S_{l_1,m_1}\left(\hat{\boldsymbol{r}}\right) S_{l_2,m_2}\left(\hat{\boldsymbol{r}}\right) S_{l,m}\left(\hat{\boldsymbol{r}}\right) \\
&= \frac{2}{\pi} \sum_{l=0}^{\infty} \sum_{m=-l}^{l} \left(-i\right)^l S_{l,m}\left(\hat{\boldsymbol{k}}\right) \int dr\, \left[r^{n_2+2} R_{n_1,l_1}\left(r\right)\right] \left(kr\right)^{-1/2} J_{l+1/2}\left(kr\right) \\
&\qquad \sum_{l_3=l_{\min}}^{l_{\max}} \sum_{m_3=-l_3}^{l_3} \left\langle l_3 m_3 \left| l_1 m_1 \right| l_2 m_2 \right\rangle_R \int d\Omega\, S_{l_3,m_3}\left(\hat{\boldsymbol{r}}\right) S_{l,m}\left(\hat{\boldsymbol{r}}\right) \qquad , \qquad \text{(A.2)} \\
&= \frac{2}{\pi} \sum_{l=0}^{\infty} \sum_{m=-l}^{l} \left(-i\right)^l S_{l,m}\left(\hat{\boldsymbol{k}}\right) \\
&\qquad \int dr\, \left[r^{n_2+2} R_{n_1,l_1}\left(r\right)\right] \left(\frac{1}{k} k\right) \left[\left(kr\right)^{\alpha} \left(kr\right)^{-\alpha}\right] \left(kr\right)^{-1/2} J_{l+1/2}\left(kr\right) \\
&\qquad \sum_{l_3=l_{\min}}^{l_{\max}} \sum_{m_3=-l_3}^{l_3} \left\langle l_3 m_3 \left| l_1 m_1 \right| l_2 m_2 \right\rangle_R \delta_{l_3,l} \delta_{m_3,m} \\
&= \frac{2}{\pi} \sum_{l_3=l_{\min}}^{l_{\max}} \sum_{m_3=-l_3}^{l_3} \left(-i\right)^{l_3} S_{l_3,m_3}\left(\hat{\boldsymbol{k}}\right) \left\langle l_3 m_3 \left| l_1 m_1 \right| l_2 m_2 \right\rangle \\
&\qquad \frac{1}{k^{\alpha+1}} \int dr\, \left[r^{n_2+2-\alpha} R_{n_1,l_1}\left(r\right)\right] k \left(kr\right)^{\alpha-1/2} J_{l_3+1/2}\left(kr\right) \\
&= \frac{2}{\pi} \sum_{l_3=l_{\min}}^{l_{\max}} \sum_{m_3=-l_3}^{l_3} \left(-i\right)^{l_3} S_{l_3,m_3}\left(\hat{\boldsymbol{k}}\right) \left\langle l_3 m_3 \left| l_1 m_1 \right| l_2 m_2 \right\rangle \frac{1}{k^{\alpha+1}} K\left(k; \alpha, n_1, l_1, n_2, l_3\right)
\end{aligned}
$$

where we have used the following definition for K:

$$K\left(k;\alpha,n_1,l_1,n_2,l_3\right)=\int dr\,\left[r^{n_2+2-\alpha}R_{n_1,l_1}\left(r\right)\right]k\left(kr\right)^{\alpha-1/2}J_{l_3+1/2}\left(kr\right). \tag{A.3}$$

Note that this definition of K allows us to apply the FFTLog algorithm since it is of the form: [29, App. B.4]

$$\int_0^\infty dr\,a\left(r\right)k\left(kr\right)^q J_\mu\left(kr\right). \tag{A.4}$$

The Fourier transform of just an orbital without the extra radial monomial and spherical harmonic is a special case of Eq. (A.2):

$$\begin{aligned}
&\mathcal{F}\left\{\phi_1\left(\boldsymbol{r}\right)\right\}\left(\boldsymbol{k}\right)\\
&=\mathcal{F}\left\{\sqrt{4\pi}\phi_1\left(\boldsymbol{r}\right)r^{n_2=0}S_{l_2=0,m_2=0}\left(\hat{\boldsymbol{r}}\right)\right\}\left(\boldsymbol{k}\right)\\
&=\sqrt{4\pi}\frac{2}{\pi}\sum_{l_3=l_{\min}}^{l_{\max}}\sum_{m_3=-l_3}^{l_3}\left(-i\right)^{l_3}\frac{1}{k^{\alpha+1}}K\left(k;\alpha,n_1,l_1,0,l_3\right)S_{l_3,m_3}\left(\hat{\boldsymbol{k}}\right)\left\langle l_3m_3\left|l_1m_1\right|0,0\right\rangle\\
&=\sqrt{4\pi}\frac{2}{\pi}\sum_{l_3=l_{\min}}^{l_{\max}}\sum_{m_3=-l_3}^{l_3}\left(-i\right)^{l_3}\frac{1}{k^{\alpha+1}}K\left(k;\alpha,n_1,l_1,0,l_3\right)S_{l_3,m_3}\left(\hat{\boldsymbol{k}}\right)\\
&\qquad\int d\Omega\,S_{l_3,m_3}\left(\hat{\boldsymbol{r}}\right)S_{l_1,m_1}\left(\hat{\boldsymbol{r}}\right)\sqrt{\frac{1}{4\pi}}\\
&=\frac{2}{\pi}\sum_{l_3=l_{\min}}^{l_{\max}}\sum_{m_3=-l_3}^{l_3}\left(-i\right)^{l_3}\frac{1}{k^{\alpha+1}}K\left(k;\alpha,n_1,l_1,0,l_3\right)S_{l_3,m_3}\left(\hat{\boldsymbol{k}}\right)\delta_{l_3,l_1}\delta_{m_3,m_1}\\
&=\frac{2}{\pi}\left(-i\right)^{l_1}\frac{1}{k^{\alpha+1}}K\left(k;\alpha,n_1,l_1\right)S_{l_1,m_1}\left(\hat{\boldsymbol{k}}\right)
\end{aligned}, \tag{A.5}$$

where

$$K\left(k;\alpha,n_1,l_1\right)=\int dr\,\left[r^{2-\alpha}R_{n_1,l_1}\left(r\right)\right]k\left(kr\right)^{\alpha-1/2}J_{l_1+1/2}\left(kr\right). \tag{A.6}$$

A.3 Overlap Integrals

$$
\begin{aligned}
&S\left(\phi_1,\phi_2;\boldsymbol{R}_1,\boldsymbol{R}_2\right)\\
&\int_{\mathbb{R}^3} d\boldsymbol{r}\,\phi_1\left(\boldsymbol{r}-\boldsymbol{R}_1\right)\phi_2\left(\boldsymbol{r}-\boldsymbol{R}_2\right)\\
&=\int_{\mathbb{R}^3} d\boldsymbol{u}\,\phi_1\left(\boldsymbol{u}\right)\phi_2\left[\boldsymbol{u}-\left(\boldsymbol{R}_2-\boldsymbol{R}_1\right)\right]\\
&=\int_{\mathbb{R}^3} d\boldsymbol{r}\,\phi_1\left(\boldsymbol{r}\right)\phi_2^*\left(\boldsymbol{r}-\boldsymbol{R}_{21}\right)\\
&=\left(2\pi\right)^{3/2}\mathcal{F}\left\{\overline{\phi_1}\left(\boldsymbol{k}\right)\overline{\phi_2}^*\left(\boldsymbol{k}\right)\right\}\left(-\boldsymbol{R}_{21}\right)\\
&=\left(2\pi\right)^{3/2}\left(2\pi\right)^{-3/2}\int_{\mathbb{R}^n} d\boldsymbol{k}\,\left[\frac{2}{\pi}\left(-i\right)^{l_1}\frac{1}{k^{\alpha+1}}K\left(k;\alpha,n_1,l_1\right)S_{l_1,m_1}\left(\hat{\boldsymbol{k}}\right)\right]\\
&\qquad\left[\frac{2}{\pi}\left(-i\right)^{l_2}\frac{1}{k^{\alpha+1}}K\left(k;\alpha,n_2,l_2\right)S_{l_2,m_2}\left(\hat{\boldsymbol{k}}\right)\right]^* e^{-i\boldsymbol{k}\cdot\left(-\boldsymbol{R}_{21}\right)}\\
&=\frac{4}{\pi^2}\left(i^2 i\right)^{l_1} i^{l_2}\int k^2 dk\,\left(\frac{1}{k^{\alpha+1}}\right)^2 K\left(k;\alpha,n_1,l_1\right)K\left(k;\alpha,n_2,l_2\right)\int d\Omega_k\,S_{l_1,m_1}\left(\hat{\boldsymbol{k}}\right)S_{l_2,m_2}\left(\hat{\boldsymbol{k}}\right)\\
&\qquad\left[4\pi\sum_{l=0}^{\infty} i^l\sqrt{\frac{\pi}{2kR_{21}}}J_{l+1/2}\left(kr_{21}\right)\sum_{m=-l}^{l} S_{l,m}\left(\hat{\boldsymbol{k}}\right)S_{l,m}\left(\hat{\boldsymbol{R}}_{21}\right)\right],\\
&=\frac{16}{\pi}\left(\frac{\pi}{2}\right)^{1/2}\sum_{l=0}^{\infty}\sum_{m=-l}^{l} i^{l+3l_1+l_2}S_{l,m}\left(\hat{\boldsymbol{R}}_{21}\right)\int d\Omega_k\,S_{l_1,m_1}\left(\hat{\boldsymbol{k}}\right)S_{l_2,m_2}\left(\hat{\boldsymbol{k}}\right)S_{l,m}\left(\hat{\boldsymbol{k}}\right)\\
&\qquad\int k^2 dk\,\left(\frac{1}{k^{\alpha+1}}\right)^2 K\left(k;\alpha,n_1,l_1\right)K\left(k;\alpha,n_2,l_2\right)\left(kR_{21}\right)^{-1/2}J_{l+1/2}\left(kR_{21}\right)\\
&=8\sqrt{\frac{2}{\pi}}\sum_{l=0}^{\infty}\sum_{m=-l}^{l} i^{l+3l_1+l_2}S_{l,m}\left(\hat{\boldsymbol{R}}_{21}\right)\\
&\qquad\sum_{l_3=l_{\min}}^{l_{\max}}\sum_{m_3=-l_3}^{l_3}\left\langle l_3 m_3\left|l_1 m_1\right|l_2 m_2\right\rangle_R\delta_{l_3,l}\delta_{m_3,m}\\
&\qquad\int k^2 dk\,\left(\frac{1}{k^{\alpha+1}}\right)^2 K\left(k;\alpha,n_1,l_1\right)K\left(k;\alpha,n_2,l_2\right)\left(kR_{21}\right)^{-1/2}J_{l+1/2}\left(kR_{21}\right)\\
&=8\sqrt{\frac{2}{\pi}}\sum_{l_3=l_{\min}}^{l_{\max}}\sum_{m_3=-l_3}^{l_3} i^{l+3l_1+l_2}S_{l_3,m_3}\left(\hat{\boldsymbol{R}}_{21}\right)\left\langle l_3 m_3\left|l_1 m_1\right|l_2 m_2\right\rangle_R\\
&\qquad\int k^2 dk\,\left(\frac{1}{k^{\alpha+1}}\right)^2 K\left(k;\alpha,n_1,l_1\right)K\left(k;\alpha,n_2,l_2\right)\left(kR_{21}\right)^{-1/2}J_{l_3+1/2}\left(kR_{21}\right)
\end{aligned}
\tag{A.7}
$$

where

$$\begin{aligned}
&\int k^2 dk \left(\frac{1}{k^{\alpha+1}}\right)^2 K\left(k;\alpha,n_1,l_1\right) K\left(k;\alpha,n_2,l_2\right) \left(kR_{21}\right)^{-1/2} J_{l_3+1/2}\left(kR_{21}\right) \\
&= \int dk \left[k^2 \left(\frac{1}{k^{\alpha+1}}\right)^2 K\left(k;\alpha,n_1,l_1\right) K\left(k;\alpha,n_2,l_2\right)\right] \left(\frac{1}{R_{21}} R_{21}\right) \\
&\quad \left[\left(kR_{21}\right)^{\beta} \left(kR_{21}\right)^{-\beta}\right] \left(kR_{21}\right)^{-1/2} J_{l_3+1/2}\left(kR_{21}\right) \\
&= \frac{1}{R_{21}^{\beta+1}} \int dk \left[k^{2-2\alpha-2-\beta} K\left(k;\alpha,n_1,l_1\right) K\left(k;\alpha,n_2,l_2\right)\right] \\
&\quad R_{21} \left(kR_{21}\right)^{\beta-1/2} J_{l_3+1/2}\left(kR_{21}\right) \\
&= \frac{1}{R_{21}^{\beta+1}} \int dk \left[k^{-2\alpha-\beta} K\left(k;\alpha,n_1,l_1\right) K\left(k;\alpha,n_2,l_2\right)\right] R_{21} \left(kR_{21}\right)^{\beta-1/2} J_{l+1/2}\left(kR_{21}\right)
\end{aligned} \quad . \quad \text{(A.8)}$$

A.4 Dipole Integrals

$$\begin{aligned}
&\boldsymbol{p}\left(\phi_1,\phi_2;\boldsymbol{R}_1,\boldsymbol{R}_2\right) \\
&= \int_{\mathbb{R}^3} \phi_1\left(\boldsymbol{r}-\boldsymbol{R}_1\right) \boldsymbol{r} \phi_2\left(\boldsymbol{r}-\boldsymbol{R}_2\right) d\boldsymbol{r} \\
&= \int_{\mathbb{R}^3} \phi_1\left(\boldsymbol{u}\right) \left(\boldsymbol{u}+\boldsymbol{R}_1\right) \phi_2\left(\boldsymbol{u}-\boldsymbol{R}_{21}\right) d\boldsymbol{u} \\
&= \boldsymbol{R}_1 \int_{\mathbb{R}^3} \phi_1\left(\boldsymbol{u}\right) \phi_{n_2 l_2 m_2}\left(\boldsymbol{u}-\boldsymbol{R}_{21}\right) d\boldsymbol{u} + \int_{\mathbb{R}^3} \phi_1\left(\boldsymbol{u}\right) \boldsymbol{u} \phi_2\left(\boldsymbol{u}-\boldsymbol{R}_{21}\right) d\boldsymbol{u} \\
&= \boldsymbol{R}_1 S\left(\phi_1,\phi_2;\boldsymbol{R}_1,\boldsymbol{R}_2\right) + \int_{\mathbb{R}^3} \phi_1\left(\boldsymbol{r}\right) x \phi_2\left(\boldsymbol{r}-\boldsymbol{R}_{21}\right) d\boldsymbol{r} \\
&\quad + \int_{\mathbb{R}^3} \phi_1\left(\boldsymbol{r}\right) y \phi_{n_2 l_2 m_2}\left(\boldsymbol{r}-\boldsymbol{R}_{21}\right) d\boldsymbol{r} + \int_{\mathbb{R}^3} \phi_1\left(\boldsymbol{r}\right) z \phi_2\left(\boldsymbol{r}-\boldsymbol{R}_{21}\right) d\boldsymbol{r} \\
&= \boldsymbol{R}_1 S\left(\phi_1,\phi_2;\boldsymbol{R}_1,\boldsymbol{R}_2\right) + \hat{x} p_x\left(\phi_1,\phi_2;\boldsymbol{R}_1,\boldsymbol{R}_2\right) \\
&\quad + \hat{y} p_y\left(\phi_1,\phi_2;\boldsymbol{R}_1,\boldsymbol{R}_2\right) + \hat{z} p_z\left(\phi_1,\phi_2;\boldsymbol{R}_1,\boldsymbol{R}_2\right)
\end{aligned}$$

where we have used the following substitution of variables: $\boldsymbol{u} = \boldsymbol{r} - \boldsymbol{R}_1 \Rightarrow d\boldsymbol{u} = d\boldsymbol{r}$ and $\mathbb{R}^3 \rightarrow \mathbb{R}^3$ and let $\boldsymbol{R}_{21} = \boldsymbol{R}_2 - \boldsymbol{R}_1$.

$$\begin{aligned} p_x\left(\phi_1,\phi_2;\boldsymbol{R}_1,\boldsymbol{R}_2\right) &= \int_{\mathbb{R}^3}\phi_1\left(\boldsymbol{r}\right)x\phi_2\left(\boldsymbol{r}-\boldsymbol{R}_{21}\right)d\boldsymbol{r} \\ &= \int_{\mathbb{R}^3}\phi_1\left(\boldsymbol{r}\right)\left[-r\sqrt{\frac{4\pi}{3}}X_1^1\left(\Omega\right)\right]\phi_2\left(\boldsymbol{r}-\boldsymbol{R}_{21}\right)d\boldsymbol{r} \\ &= -\sqrt{\frac{4\pi}{3}}\int_{\mathbb{R}^3}\phi_1\left(\boldsymbol{r}\right)r^1X_1^1\left(\Omega\right)\phi_2\left(\boldsymbol{r}-\boldsymbol{R}_{21}\right)d\boldsymbol{r} \\ &= -\sqrt{\frac{4\pi}{3}}G\left(\phi_1,\phi_2;\boldsymbol{R}_{21},1,1,1\right) \end{aligned}$$

$$\begin{aligned} p_y\left(\phi_1,\phi_2;\boldsymbol{R}_1,\boldsymbol{R}_2\right) &= \int_{\mathbb{R}^3}\phi_1\left(\boldsymbol{r}\right)y\phi_2\left(\boldsymbol{r}-\boldsymbol{R}_{21}\right)d\boldsymbol{r} \\ &= \int_{\mathbb{R}^3}\phi_1\left(\boldsymbol{r}\right)\left[-r\sqrt{\frac{4\pi}{3}}X_1^{-1}\left(\Omega\right)\right]\phi_2\left(\boldsymbol{r}-\boldsymbol{R}_{21}\right)d\boldsymbol{r} \\ &= -\sqrt{\frac{4\pi}{3}}\int_{\mathbb{R}^3}\phi_1\left(\boldsymbol{r}\right)r^1X_1^{-1}\left(\Omega\right)\phi_2\left(\boldsymbol{r}-\boldsymbol{R}_{21}\right)d\boldsymbol{r} \\ &= -\sqrt{\frac{4\pi}{3}}G\left(\phi_1,\phi_2;\boldsymbol{R}_{21},1,1,-1\right) \end{aligned}$$

$$\begin{aligned} p_z\left(\phi_1,\phi_2;\boldsymbol{R}_1,\boldsymbol{R}_2\right) &= \int_{\mathbb{R}^3}\phi_1\left(\boldsymbol{r}\right)z\phi_2\left(\boldsymbol{r}-\boldsymbol{R}_{21}\right)d\boldsymbol{r} \\ &= \int_{\mathbb{R}^3}\phi_1\left(\boldsymbol{r}\right)\left[-r\sqrt{\frac{4\pi}{3}}X_1^0\left(\Omega\right)\right]\phi_2\left(\boldsymbol{r}-\boldsymbol{R}_{21}\right)d\boldsymbol{r} \\ &= -\sqrt{\frac{4\pi}{3}}\int_{\mathbb{R}^3}\phi_1\left(\boldsymbol{r}\right)r^1X_1^0\left(\Omega\right)\phi_2\left(\boldsymbol{r}-\boldsymbol{R}_{21}\right)d\boldsymbol{r} \\ &= -\sqrt{\frac{4\pi}{3}}G\left(\phi_1,\phi_2;\boldsymbol{R}_{21},1,1,0\right) \end{aligned}$$

where G is derived below:

$$
\begin{aligned}
&G\left(\phi_1,\phi_2;\boldsymbol{R}_{21},n,l,m\right)\\
&=\int_{\mathbb{R}^3}d\boldsymbol{r}\,\phi_1\left(\boldsymbol{r}\right)r^nX_l^m\phi_2\left(\boldsymbol{r}-\boldsymbol{R}_{21}\right)\\
&=\int_{\mathbb{R}^3}d\boldsymbol{r}\,\phi_1\left(\boldsymbol{r}\right)r^nX_l^m\phi_2\left(\boldsymbol{r}-\boldsymbol{R}_{21}\right)\\
&=\left(2\pi\right)^{3/2}\left\{\left(2\pi\right)^{-3/2}\int_{\mathbb{R}^3}\left[\phi_1\left(\boldsymbol{r}\right)r^nX_l^m\left(\Omega\right)\right]\phi_2\left(\boldsymbol{r}-\boldsymbol{R}_{21}\right)\right\}\\
&=\left(2\pi\right)^{3/2}\left(\phi_1r^nX_l^m\hat{*}\phi_2\right)\left(\boldsymbol{R}_{21}\right)\\
&=\left(2\pi\right)^{3/2}\mathcal{F}^{-1}\left\{\mathcal{F}\left\{\phi_1\left(\boldsymbol{r}\right)r^nX_l^m\left(\Omega\right)\right\}\left(\boldsymbol{k}\right)\mathcal{F}^{-1}\left\{\phi_2\left(\boldsymbol{r}\right)\right\}\left(\boldsymbol{k}\right)\right\}\left(\boldsymbol{R}_{21}\right)\\
&=\left(2\pi\right)^{3/2}\left(2\pi\right)^{-3/2}\int_{\mathbb{R}^3}d\boldsymbol{k}\,\sqrt{\frac{2}{\pi}}i^lX_{l_2}^{m_2}\left(\Omega_k\right)K_{n_2l_2}\left(k\right)e^{i\boldsymbol{k}\cdot\boldsymbol{R}_{21}}\\
&\qquad\sqrt{\frac{2}{\pi}}\sum_{l'=l_{min}}^{l_1+l}\sum_{m=-l'}^{l'}\left(-i\right)^{l'}X_{l'}^{m'}\left(\Omega_k\right)K_{n_1l_1}\left(k;n\right)\left\langle l'm',l_1m_1,lm\right\rangle_R\\
&=\frac{2}{\pi}\sum_{l'=l_{min}}^{l_1+l}\sum_{m=-l'}^{l'}\left(-i\right)^{l'}\left\langle l'm',l_1m_1,lm\right\rangle_R\int_{\mathbb{R}^3}d\boldsymbol{k}\,K_{n_2l_2}\left(k\right)K_{n_1l_1}\left(k;n\right)\\
&\qquad X_{l'}^{m'}\left(\Omega_k\right)\left[4\pi\sum_{l''=0}^{\infty}\sum_{m=-l''}^{l''}i^{l''}j_{l''}\left(kR_{21}\right)X_{l''}^{m''}\left(\Omega_k\right)X_{l''}^{m''}\left(\Omega_{21}\right)\right]\\
&=8\sum_{l'=l_{min}}^{l_1+l}\sum_{m=-l'}^{l'}\left(-1\right)^{l'}i^{l'+l''}\left\langle l'm',l_1m_1,lm\right\rangle_R\\
&\qquad\sum_{l''=0}^{\infty}\sum_{m=-l''}^{l''}X_{l''}^{m''}\left(\Omega_{21}\right)\int d\Omega_k\,X_{l''}^{m''}\left(\Omega_k\right)X_{l'}^{m'}\left(\Omega_k\right)\\
&\qquad\int k^2dk\,K_{n_2l_2}\left(k\right)K_{n_1l_1}\left(k;n\right)j_{l''}\left(kR_{21}\right)\\
&=8\sum_{l'=l_{min}}^{l_1+l}\sum_{m=-l'}^{l'}i^{-l'+l''}\left\langle l'm',l_1m_1,lm\right\rangle_R\\
&\qquad\sum_{l''=l''_{min}}^{\infty}\sum_{m=-l''}^{l''}X_{l''}^{m''}\left(\Omega_{21}\right)\delta_{l'',l'}\delta_{m'',m'}\\
&\qquad\int k^2dk\,K_{n_2l_2}\left(k\right)K_{n_1l_1}\left(k;n\right)j_{l''}\left(kR_{21}\right)
\end{aligned}
$$

$$= 8 \sum_{l'=l_{min}}^{l_1+l} \sum_{m=-l'}^{l'} i^{-l'+l''} \left\langle l'm', l_1m_1, lm \right\rangle_R X_{l'}^{m'} \left(\Omega_{21}\right)$$
$$\int k^2 dk \, K_{n_2l_2}\left(k\right) K_{n_1l_1}\left(k;n\right) j_{l'}\left(kR_{21}\right)$$

A.5 Momentum Integrals

$$\begin{aligned}
&\partial x \left(\phi_1, \phi_2; \boldsymbol{R}_1, \boldsymbol{R}_2\right) \\
&= \int_{\mathbb{R}^3} \phi_1 \left(\boldsymbol{x} - \boldsymbol{R}_1\right) \frac{\partial}{\partial x} \phi_2 \left(\boldsymbol{x} - \boldsymbol{R}_2\right) d\boldsymbol{x} \\
&= D \left(\phi_1, \phi_2; \boldsymbol{R}_1, \boldsymbol{R}_2, 1, 1\right) \\
&= 8 \sum_{l=0}^{\infty} \sum_{m=-l}^{l} i^{n-l_1+l_2+l} X_l^m \left(\Omega_{12}\right) \int d\Omega_k \, X_l^m \left(\Omega_k\right) X_{l_1}^{m_1} \left(\Omega_k\right) X_{l_2}^{m_2} \left(\Omega_k\right) \\
&\quad \int dk \, j_l \left(kR_{12}\right) K_{n_1l_1} \left(k\right) K_{n_2l_2} \left(k\right) k_x \\
&= 8 \sum_{l=0}^{\infty} \sum_{m=-l}^{l} i^{n-l_1+l_2+l} X_l^m \left(\Omega_{12}\right) \int d\Omega_k \, X_l^m \left(\Omega_{12}\right) X_{l_1}^{m_1} \left(\Omega_k\right) X_{l_2}^{m_2} \left(\Omega_k\right) \\
&\quad \int k^2 dk \, j_l \left(kR_{12}\right) K_{n_1l_1} \left(k\right) K_{n_2l_2} \left(k\right) \left[-k\sqrt{\frac{4\pi}{3}} X_1^1 \left(\Omega_k\right)\right] \\
&= -8\sqrt{\frac{4\pi}{3}} \sum_{l=0}^{\infty} \sum_{m=-l}^{l} i^{n-l_1+l_2+l} X_l^m \left(\Omega_{12}\right) \int d\Omega_k \, X_l^m \left(\Omega_k\right) X_{l_1}^{m_1} \left(\Omega_k\right) X_{l_2}^{m_2} \left(\Omega_k\right) X_1^1 \left(\Omega_k\right) \\
&\quad \int k^2 dk \, k j_l \left(kR_{12}\right) K_{n_1l_1} \left(k\right) K_{n_2l_2} \left(k\right) \\
&= -8\sqrt{\frac{4\pi}{3}} \sum_{l=lmin}^{lmax} \sum_{m=-l}^{l} i^{n-l_1+l_2+l} X_l^m \left(\Omega_{12}\right) \left\langle lm, l_1m_1, l_2m_2, 11 \right\rangle_R \\
&\quad \int k^2 dk \, k j_l \left(kR_{12}\right) K_{n_1l_1} \left(k\right) K_{n_2l_2} \left(k\right)
\end{aligned}$$

In the above derivation we make use of the following equalities: $k_x = -k\sqrt{\frac{4\pi}{3}} X_1^1 \left(\Omega_k\right)$, $k_y = -k\sqrt{\frac{4\pi}{3}} X_1^{-1} \left(\Omega_k\right)$, and $k_z = k\sqrt{\frac{4\pi}{3}} X_1^0 \left(\Omega_k\right)$.

$$
\begin{aligned}
&D\left(\phi_1,\phi_2;\boldsymbol{R}_1,\boldsymbol{R}_2,i,n\right)\\
&=\int_{\mathbb{R}^3}\phi_1\left(\boldsymbol{x}-\boldsymbol{R}_1\right)\frac{\partial^n}{\partial x_i^n}\phi_2\left(\boldsymbol{x}-\boldsymbol{R}_2\right)d\boldsymbol{x}\\
&=\int_{\mathbb{R}^3}\phi_1\left(\boldsymbol{u}-\boldsymbol{R}_{12}\right)\frac{\partial^n}{\partial u_i^n}\phi_2\left(\boldsymbol{u}\right)d\boldsymbol{r}\\
&=\left(2\pi\right)^{3/2}\left\{\left(2\pi\right)^{-3/2}\int_{\mathbb{R}^3}\left[\frac{\partial^n}{\partial u_i^n}\phi_2\left(\boldsymbol{u}\right)\right]\phi_1\left(\boldsymbol{u}-\boldsymbol{R}_{12}\right)d\boldsymbol{u}\right\}\\
&=\left(2\pi\right)^{3/2}\left(\frac{\partial^n}{\partial u_i^n}\phi_2\hat{*}\phi_1\right)\left(\boldsymbol{R}_{12}\right)\\
&=\left(2\pi\right)^{3/2}\mathcal{F}^{-1}\left\{\mathcal{F}\left\{\frac{\partial^n}{\partial u_i^n}\phi_2\left(\boldsymbol{u}\right)\right\}\left(\boldsymbol{k}\right)\mathcal{F}^{-1}\left\{\phi_1\left(\boldsymbol{r}\right)\right\}\left(\boldsymbol{k}\right)\right\}\left(\boldsymbol{R}_{12}\right)\\
&=\left(2\pi\right)^{3/2}\mathcal{F}^{-1}\left\{\left(ik_i\right)^n\mathcal{F}\left\{\phi_2\left(\boldsymbol{u}\right)\right\}\left(\boldsymbol{k}\right)\mathcal{F}^{-1}\left\{\phi_1\left(\boldsymbol{r}\right)\right\}\left(\boldsymbol{k}\right)\right\}\left(\boldsymbol{R}_{12}\right)\\
&=\left(2\pi\right)^{3/2}\left(2\pi\right)^{-3/2}\int d\boldsymbol{k}\,e^{i\boldsymbol{k}\cdot\boldsymbol{R}_{12}}\left(ik_i\right)^n\sqrt{\frac{2}{\pi}}i^{l_2}X_{l_2}^{m_2}\left(\Omega_k\right)K_{n_2l_2}\left(k\right)\\
&\quad\sqrt{\frac{2}{\pi}}\left(-i\right)^{l_1}X_{l_1}^{m_1}\left(\Omega_k\right)K_{n_1l_1}\left(k\right)\\
&=\frac{2}{\pi}i^{n+l_1+l_2}\left(-1\right)^{l_1}\int d\boldsymbol{k}\,k_i^n\left[4\pi\sum_{l=0}^{\infty}\sum_{m=-l}^{l}i^l j_l\left(kR_{12}\right)X_l^m\left(\Omega_k\right)X_l^m\left(\Omega_{12}\right)\right]\\
&\quad X_{l_2}^{m_2}\left(\Omega_k\right)K_{n_2l_2}\left(k\right)X_{l_1}^{m_1}\left(\Omega_k\right)K_{n_1l_1}\left(k\right)\\
&=8\sum_{l=0}^{\infty}\sum_{m=-l}^{l}i^{n-l_1+l_2+l}X_l^m\left(\Omega_{12}\right)\int d\Omega_k\,X_l^m\left(\Omega_k\right)X_{l_1}^{m_1}\left(\Omega_k\right)X_{l_2}^{m_2}\left(\Omega_k\right)\\
&\quad\int k^2dk\,j_l\left(kR_{12}\right)K_{n_1l_1}\left(k\right)K_{n_2l_2}\left(k\right)k_i^n
\end{aligned}
$$

, where we made the following change of variables: $\boldsymbol{u}=\boldsymbol{x}-\boldsymbol{R}_2\Rightarrow du_i=dx_i$ so that $\frac{\partial}{\partial x_i}=\frac{\partial}{\partial u_i}\frac{\partial u_i}{\partial x_i}=\frac{\partial}{\partial u_i}$ and let $\boldsymbol{R}_{12}=\boldsymbol{R}_1-\boldsymbol{R}_2$. Also, $i^{n+l_1+l_2}\left(-1\right)^{l_1}=i^{n+l_1+l_2}i^{2l_1}=i^{n+3l_1+2l_2}=i^{n-l_1+l_2}$.

A.6 Kinetic Integrals

The kinetic integrals follow immediately from repeated use of D in the derivation of the momentum integrals:

$$\begin{aligned} & T\left(\phi_1, \phi_2; \boldsymbol{R}_1, \boldsymbol{R}_2\right) \\ & = \int_{\mathbb{R}^3} \phi_1\left(\boldsymbol{x} - \boldsymbol{R}_1\right) \boldsymbol{\nabla}^2 \phi_2\left(\boldsymbol{x} - \boldsymbol{R}_2\right) d\boldsymbol{x} \\ & = D\left(\phi_1, \phi_2; \boldsymbol{R}_1, \boldsymbol{R}_2, 1, 2\right) + D\left(\phi_1, \phi_2; \boldsymbol{R}_1, \boldsymbol{R}_2, 2, 2\right) + D\left(\phi_1, \phi_2; \boldsymbol{R}_1, \boldsymbol{R}_2, 1, 3\right) \end{aligned} \tag{A.9}$$

Glossary

ALDA adiabatic local density approximation. 13, 20, 29

DFT density functional theory. 1, 8–13, 15, 16, 20, 29

FFT Fast Fourier Transform. 26, 36

FFTLog Logarithmic Fast Fourier Transform. 26, 36, 37, 44

GGA generalized gradient approximation. 11

GTO Gaussian-type Orbital. 30, 36

LDA local density approximation. 11, 17, 29

optical frequency a frequency in the electromagnetic spectrum near 10^{15} Hz and corresponding to a wavelength of about 10^{-6} m [**?**, Page 377]. 1

TDCDFT time-dependent current density functional theory. 1, 2, 14–17, 19, 21, 27, 29, 36, 37

TDDFT time-dependent density functional theory. 12, 13, 17

Index